Tectonic controls on sediment provenance evolution in rift basins: Detrital zircon U–Pb and Hf isotope analysis from the Perth Basin, Western Australia

Hugo K.H. Olierook, Milo Barham, Ian C.W. Fitzsimons, Nicholas E. Timms, Qiang Jiang, Noreen J. Evans, Bradley J. McDonald

PII: S1342-937X(18)30257-0
DOI: https://doi.org/10.1016/j.gr.2018.11.002
Reference: GR 2036

To appear in: *Gondwana Research*

Received date: 18 June 2018
Revised date: 25 September 2018
Accepted date: 5 November 2018

Please cite this article as: Hugo K.H. Olierook, Milo Barham, Ian C.W. Fitzsimons, Nicholas E. Timms, Qiang Jiang, Noreen J. Evans, Bradley J. McDonald , Tectonic controls on sediment provenance evolution in rift basins: Detrital zircon U–Pb and Hf isotope analysis from the Perth Basin, Western Australia. Gr (2018), https://doi.org/10.1016/j.gr.2018.11.002

Tectonic controls on sediment provenance evolution in rift basins: detrital zircon U–Pb and Hf isotope analysis from the Perth Basin, Western Australia

Hugo K. H. Olierook[1,*], Milo Barham[1,2], Ian C. W. Fitzsimons[1], Nicholas E. Timms[1], Qiang Jiang[1], Noreen J. Evans[1,3], Bradley J. McDonald[3]

[1]School of Earth and Planetary Sciences, Curtin University, GPO Box U1987, Perth, WA 6845, Australia

[2]Centre for Exploration and Targeting, Curtin University, GPO Box U1987, Perth, WA 6845, Australia

[3]John de Laeter Centre, Curtin University, GPO Box U1987, Perth, WA 6845, Australia

*Compiled by / corresponding author: hugo.olierook@curtin.edu.au; +61 8 9266 7827

Keywords: continental breakup; drainage; U–Pb geochronology; Yilgarn Craton; Gondwana

Abstract

The role of tectonics in controlling temporal and spatial variations in sediment provenance during the evolution of extensional basins from initial rifting to continental breakup and passive margin development are not well established. We test the influence of tectonics in a rift basin that has experienced minimal uplift but significant extension throughout its history: the Perth Basin, Western Australia. We use published zircon U–Pb and Hf isotope data from basin inception through to continental drift and complement this with new data from samples deposited synchronously with the continental breakup of eastern Gondwana. Three primary source regions are inferred, namely the Archean Yilgarn Craton to the east, the Paleo- and Mesoproterozoic Albany–Fraser–Wilkes Orogen to the south and east, and the Mesoproterozoic and Ediacaran–Cambrian Pinjarra Orogen underlying the rift basin and comprising the dominant crustal components to the west and southwest. From mid-Paleozoic basin inception to Early Cretaceous breakup of eastern Gondwana, drainage in the Perth Basin was primarily north- to northwest-directed as evidenced by the dominant Mesoproterozoic detrital zircon cargo, paleodrainage patterns and paleocurrent directions. Thus, provenance was primarily parallel to the rift axis and perpendicular to the extension direction, particularly during periods of thermal subsidence. During episodes of mechanical extension, detrital zircon ages are polymodal and consistently dominated by Paleo- and Mesoproterozoic grains derived from the Albany–Fraser–Wilkes Orogen, but with significant Archean and Neoproterozoic inputs from the rift margins. It is inferred that during mechanical extension the rate of subsidence exceeded sediment supply, which generated basin-margin scarps and enhanced direct input from the rift shoulders. Detrital zircon spectra from temporally-equivalent samples at the rift margin and in the rift axis reveal that distinct sedimentary routing operated on the flanks. In summary, sediment provenance in the Perth Basin (and probably other rift basins) is tectonically controlled by: (1) extension direction, (2) episodes of mechanical extension (rift) or thermal subsidence (post-rift), and (3) proximity to rift axis or rift margin.

1 INTRODUCTION

Sediment provenance studies are concerned with the location and nature of sediment source areas, the pathways by which sediment is transferred from source to sink, and the factors that influence the composition of sedimentary rocks (Fig. 1; Haughton et al., 1991; Weltje and von Eynatten, 2004). Determining provenance in sedimentary basins via U–Pb detrital zircon geochronology can play a critical role in assessing plate tectonic reconstructions (Cawood et al., 2013; Gehrels, 2014), characterizing crust which is no longer exposed or preserved (Glen et al., 2017; Markwitz et al., 2017a), testing tectonic models for uplift and subsidence at local or epeirogenic scales (Bush et al., 2016; Moecher et al., 2018; Shao et al., 2016), mapping depositional systems (Barham et al., 2018), understanding paleodrainage systems (Horton et al., 2015) and predicting reservoir quality (Vincent et al., 2013). In convergent tectonic settings, sediment sources tend to be proximal to the orogenic front and often correspond to newly formed continental crust (Cawood et al., 2012; Dickinson and Suczek, 1979). Conversely, sediment sources in extensional settings tend to be significantly older than the rift axis and sediment transport distances may be significantly longer (Cawood et al., 2012). Constraining the controls on provenance in extensional settings is particularly important for understanding the processes involved during rifting and the eventual breakup of supercontinents.

There are numerous intrinsic and extrinsic factors that limit our ability to effectively reconstruct the origin and transport history of sediments from a basin fill (Fig. 1). The use of zircon in detrital provenance studies significantly reduces the impact of many of these factors as a consequence of its physical robustness and geochemical fidelity. Whilst significant compositional information of parental sources may be lost through the action of various processes during sediment transport, deposition and diagenesis, zircon isotope signatures elucidate the fundamental geological processes that link detrital material in sedimentary rocks to their primary source region(s) (Gehrels, 2014). Therefore, the use of zircon isotopic data is, arguably, the gold standard in reconstructing detrital contributions from

various source terranes to basin fill material. In turn, the ability to resolve source region contributions has implications for understanding sediment transport pathways and the factors that control their distribution and efficiency.

In this study, we specifically aim to understand the role of extension on sediment provenance through space and time in rift basins using zircon isotope systematics. The Perth Basin in Western Australia is an archetypal rift basin for investigating provenance systematics because it typifies important aspects of major rift basins worldwide and allows us to constrain several major factors that influence sediment provenance (Fig. 1).

(i) The Perth Basin is large in spatial extent (~150 × 800 km) with a protracted history, recording a mid-Paleozoic to Early Cretaceous rift succession that culminated with the continental breakup of eastern Gondwana at ca. 137–136 Ma (Gibbons et al., 2012; Olierook et al., 2015b). The size and longevity of the Perth Basin permit the study of variations in provenance over long distances and time frames.

(ii) The transport mechanism throughout the majority of the Perth Basin was dominated by fluvial systems, reducing the influence of marine processes, relative sea level effects and transport media (e.g., water, wind) on provenance considerations (Crostella and Backhouse, 2000; Mory and Iasky, 1996; Olierook et al., 2015b). Some Late Permian–Early Triassic and Middle Jurassic shallow marine incursions exist and some glacigene sedimentary rocks from the Early Permian (late Paleozoic ice age) also occur but these are subordinate to the fluviatile regime that operated during the rest of the Perth Basin history.

(iii) The Perth Basin was drained from several crystalline basement blocks that are dominated by felsic rocks that have distinct ages and histories, making it possible to assess provenance using zircon isotope data and curtailing the influence of different rock type sources (Cawood and

Nemchin, 2000; Spencer et al., in press). Although differences in zircon fertility might bias the contributions of the different granitoid terranes, and very minor metasedimentary terranes exist in one part of the basin periphery (Northampton Complex; Ksienzyk et al., 2012), it is still viable to track relative contributions in source terranes through time in a basin (McLennan et al., 1993; Moecher and Samson, 2006). Moreover, the differences in zircon fertility between different granitoid terranes are insignificant compared to a basin that has sourced its fill from varied rock types.

(iv) The Perth Basin endured multiple discrete episodes of rifting with high rates of mechanical extension (rifting) interspersed by periods of thermal subsidence with lower rates of extension but it experienced relatively little intrabasinal exhumation before continental breakup in the Early Cretaceous (Olierook and Timms, 2016). The paucity of pre-breakup intrabasinal exhumation significantly restricts the influence of intrabasinal sediment recycling (Green and Duddy, 2013; Olierook and Timms, 2016).

(v) Southwestern Australia and adjacent continental blocks experienced warm to cool temperate regimes from the middle Permian to Early Cretaceous, thereby sustaining perennial fluvial activity and maintaining similar transport media (Boucot et al., 2013; Scotese et al., 2014). Climate in Western Australia was only a significant variable for the Early Permian (late Paleozoic ice age, Nangetty Formation), for which no zircon U–Pb data currently exist, and for the oldest rocks in the basin – the mid-Paleozoic Tumblagooda Sandstone – when arid conditions were experienced by adjacent source terranes (Eyles et al., 2006; Hocking, 1991).

(vi) Previous studies of the Perth Basin have generated substantial zircon U–Pb and Hf isotopic data although they have not previously been synthesised in the context of whole-basin processes (Cawood and Nemchin, 2000; Dillinger et al., 2018; Lewis, 2017; Markwitz et al., 2017c; Sircombe and Freeman, 1999).

(vii) Published paleocurrent, paleodrainage and basin fill data for the Perth Basin help constrain provenance directions (Mory and Iasky, 1996; Olierook et al., 2015a; Olierook et al., 2015b).

To test the effects of regional tectonics on detrital sediment supply from distinct source regions to different parts of the Perth Basin, we have compiled published detrital zircon U–Pb and Hf isotope data from the syn-rift and post-breakup successions in the Perth Basin, and complemented this with new data from samples that straddle the breakup unconformity, which is a period previously lacking published detrital zircon data. We assess the tectonic influence on source rock exhumation and transport pathways, with particular emphasis on the interplay of axial and transverse drainage systems but also the effect of sub-basin compartmentalization and the capacity for effective mixing of different sources. Finally, we demonstrate the importance of continental breakup – a change in tectonic setting – in irrevocably altering the sediment provenance signature of the Perth Basin.

2 GEOLOGICAL HISTORY

2.1 Assembly of eastern Gondwana

The amalgamation of eastern Gondwana resulted from the juxtaposition of Indo–Antarctic and Australo–Antarctic continents during the late Neoproterozoic and early Cambrian (Fig. 2; Aitken et al., 2016; Aitken et al., 2014; Boger, 2011; Boger and Miller, 2004; Collins and Pisarevsky, 2005; Daczko et al., 2018; Fitzsimons, 2000, 2003; Meert and van der Voo, 1997; Meert et al., 1995; Merdith et al., 2017; Myers et al., 1996; Schmitt et al., 2018). Paleomagnetic data reveal that Australo-Antarctica and Indo-Antarctica were separated by >20° latitude at ca. 770–750 Ma (Gregory et al., 2009; Torsvik et al., 2001; Wingate and Giddings, 2000). Although no direct evidence for a suture zone has been found to date, some 3000–5000 km of relative plate motion between Indo-Antarctica and Australo-Antarctica was required for final Gondwana amalgamation at ca. 550–500

Ma (Gregory et al., 2009; Halpin et al., 2017; Li et al., 2013). Several terms have been used for this Ediacaran–Cambrian orogenic event and its geographic extent. The Indo–Antarctic and Australo–Antarctic collisional event has been called the Kuunga Orogeny (Aitken et al., 2016; Aitken et al., 2014; Boger, 2011; Boger and Miller, 2004; Meert, 2003; Meert et al., 1995) or the Pinjarra Orogeny (Fitzsimons, 2000, 2003; Veevers and Saeed, 2011), and the Kuunga Orogeny is used in this study. The geographic location of amalgamation has been termed the Kuunga Orogen/Suture (Boger, 2011; Boger and Miller, 2004; Meert, 2003; Meert et al., 1995), the Pinjarra Orogen (Fitzsimons, 2003), the Prydz-Denman-Darling Orogen (Fitzsimons, 2000) or the Indo-Australo-Antarctic Suture (Aitken et al., 2016; Aitken et al., 2014), and we use the Pinjarra Orogen here to encompass the wider orogenic belt. The precise extent of the Pinjarra Orogen is still uncertain because the sediments and sedimentary rocks of the Perth Basin cover most of the orogen in Australia, in Antarctica it is almost entirely blanketed by ice sheets, and its correlative rocks in parts of Greater India are now subducted under Asia (Aitken et al., 2014; Capitanio et al., 2010; Olierook et al., 2015b). Finally, the term Pinjarra Orogeny has been used for the ca. 1090–1020 Ma orogenic event that affected the western margin of Australia (Boger, 2011; Ksienzyk et al., 2012; Wilde, 1999), which is adopted here.

2.2 Rifting and breakup of eastern Gondwana, and the formation of the Perth Basin

The Perth Basin is ~800 km long × 150 km wide, representing the eastern half of an Indian–Australian rift basin along which the breakup of eastern Gondwana was focussed (Fig. 3; Olierook et al., 2015b). Rifting of eastern Gondwana commenced by at least the mid-Paleozoic, as evidenced by the onset of sedimentation in the northern Perth Basin (Tumbalgooda Sandstone; Harris, 1994; Olierook et al., 2015b; Playford et al., 1976). The locus of rifting was approximately coincident with the eastern margin of the Pinjarra Orogen (Halpin et al., 2017), implying that the Ediacaran–Cambrian suture was probably to the west of the Perth Basin. Alternatively, as orogens commonly record multiple suture zones (Replumaz et al., 2010; Yang et al., 2003), more than one suture could have

been present in the Pinjarra Orogen and the Perth Basin simply exploited the lithospheric weakness of an eastern suture. Regardless of which scenario is correct, rifting occurred approximately geographically coincident to the Ediacaran–Cambrian orogenic front.

The Perth Basin records at least four distinct episodes of mechanical extension (rift) in the mid-Paleozoic, Permian, Early Jurassic and Late Jurassic–Early Cretaceous (Fig. 3; Hocking, 1991; Song and Cawood, 2000). The last of these rifting events served as the trigger for continental breakup of India and Australia–Antarctica (Gibbons et al., 2013). The final stages of continental breakup may have been thermally aided by the impingement and incubation of the Kerguelen mantle plume from ca. 147–140 Ma (Olierook et al., 2017 and references therein; Shi et al., 2018). The timing of ultimate breakup of eastern Gondwana along the west Australian margin has been constrained to ca. 137–136 Ma using recent plate reconstructions and palynological biozones from underlying strata (Gibbons et al., 2013; Jones et al., 2012).

The conjugate margin in Greater India is now subducted beneath the Himalayas and is, therefore, inaccessible (Capitanio et al., 2010). Paleocurrent data and paleodrainage reconstruction maps show that drainage was primarily directed northward to northwestward for the entire length and duration of the pre-breakup Perth Basin, with minor tributaries encroaching onto the Yilgarn Craton in the east during episodes of mechanical extension (Eyles et al., 2006; Hocking, 1991; Mory and Iasky, 1996; Olierook et al., 2015a; Wilde and Walker, 1977). Depositional facies along the entire length of the Perth Basin were almost exclusively fluviatile prior to continental breakup, with the exception of glacigene facies in the Early Permian and minor marine incursions in the Late Permian–Early Triassic and Middle Jurassic (Eyles et al., 2006; Mory and Iasky, 1996).

During continental breakup, lava flows known as the Bunbury Basalt erupted onto the breakup unconformity within the north–south striking Bunbury Trough in the southern Perth Basin (Olierook et al., 2015a). The Bunbury Basalt has been dated at 137–130 Ma (Coffin et al., 2002; Olierook et al.,

2016), with the earliest eruptions concomitant with the breakup of India and Australia–Antarctica (Gibbons et al., 2012; Jones et al., 2012). The Bunbury Basalt was extruded as at least three distinct flows into two deeply-incised axially-draining paleovalleys (Olierook et al., 2015a).

Since continental breakup, the onshore Perth Basin has accumulated relatively little preserved sedimentary fill (Olierook and Timms, 2016). Sediment deposition has been refocussed to the offshore Perth Basin – what has now become the eastern Indian Ocean – with the transition to the modern day passive margin of Western Australia.

3 METHODS

3.1 Compilation of previous detrital zircon U–Pb and Hf isotopic data from the Perth Basin

All previously published detrital zircon U–Pb and Hf isotopic data for detrital zircon grains from the Perth Basin were compiled in a new dataset that may be found, together with new sample data, in supplementary Table A. The full dataset includes detrital zircon data from 46 samples, 2435 U–Pb analyses with <10 % discordance and 437 Hf isotopic data on the same spots as the U–Pb analyses (Cawood and Nemchin, 2000; Dillinger et al., 2018; Lewis, 2017; Markwitz et al., 2017c; Sircombe and Freeman, 1999; Veevers et al., 2005). Spatially, detrital samples are dominantly from the northern Perth Basin and, with new data, from the southern Perth Basin (Fig. 3). Temporally, detrital zircon samples range from the mid-Paleozoic basin inception (Tumblagooda Sandstone) to modern-day beach sediments along the Western Australian coastline. Significant gaps in the data exist in the central Perth Basin and in the Jurassic (Fig. 3) but further work is currently underway to fill this gap in knowledge (Fig. 3; Len Baddock 2018, writ. comms).

3.2 New sample selection

Three samples of sandstone were selected from two drill cores that intersected flows of Bunbury Basalt, stored in the Perth Core Library of the Geological Survey of Western Australia (Table 1). Two samples were collected from Donnybrook Drill Bore DDB7 proximal to the basin margin (samples 7A & 7B, point **r** in Fig. 3), located above and below a single, ~70 m flow of Bunbury Basalt in the Donnybrook Paleovalley dated at 135.9 ± 1.0 Ma (Morant, 1988; Olierook et al., 2015a). Paleontological work has not been undertaken on these samples but it is likely that the lower and upper samples correspond to the earliest Cretaceous Parmelia Group (Backhouse, 1988). Sample 7A is a beige, argillaceous, moderately-cemented, coarse-grained sandstone. Grain clasts are subangular to subrounded and comprise chiefly of quartz, minor feldspar and rare zircon and opaque minerals. Sample 7B is a light grey, well-consolidated, very coarse-grained sandstone with occasional granules. Grain clasts comprise chiefly of clean, subangular to subrounded quartz with rare pyrite, feldspar, zircon, biotite and hornblende.

One sample was collected from Bunbury Hole BH14 (point **q** in Fig. 3) located within the basin axis between two lava flows in the Bunbury Paleovalley (Olierook et al., 2015a). Recent palynological work on the interflow sample shows that this unit belongs to the Parmelia Group (Ibilola, 2017), the final pre-breakup sedimentary succession in the Perth Basin. Sample BH14 is a grey, argillaceous, moderately-cemented, fine-grained sandstone. Grain clasts comprise chiefly of quartz, with minor feldspar and rare muscovite and biotite.

3.3 New sample preparation and grain imaging

All three samples were disaggregated using the SelFrag electric pulse fragmenter in the John de Laeter Centre (JdLC) at Curtin University to liberate their constituent minerals. Heavy mineral fractions were separated using standard techniques, all zircon grains were mounted in 25 mm diameter epoxy stubs and polished to half-grain thickness to expose their interiors. Mounted grains were imaged with transmitted and reflected light on an optical microscope and, subsequently, with back-

scattered electron (BSE) and cathodoluminescence (CL) imaging using a Tescan Mira3 FEG-SEM at the JdLC at Curtin University. Transmitted and reflected light images were used to assess grain shape and transparency. BSE and CL images were used to document internal zonation patterns (e.g. oscillatory, sector) and identify growth and recrystallization textures (Corfu et al., 2003).

3.4 Zircon U–Th–Pb and Lu–Hf isotopic data

Zircon U–Th–Pb and Lu–Hf isotopic measurements were collected simultaneously using the laser ablation split stream system housed in the GeoHistory Facility, JdLC, Curtin University. Where possible, multiple spots were collected from both grain cores and rims. Analyses were conducted targeting sufficient grains to represent minor subpopulations without preselecting grains, in order to minimise sample bias and yield an objective detrital zircon distribution (Vermeesch, 2004). An overview of operating conditions is given here but more detail can be found in Spencer et al. (2017). The excimer laser (Resonetics S-155-LR 193 nm) spot diameters were 30 and 50 µm, laser fluence was 2 J cm^{-2} with a repetition rate of 5 Hz for 30 seconds of total of analysis time and ~50 seconds of background capture. All analyses were preceded by two cleaning pulses. The sample cell was flushed by ultrahigh purity He (0.68 L min^{-1}) and N_2 (2.8 mL min^{-1}). Importantly, analytical results from two different spot diameters (30 and 50 µm) show negligible variation in detrital zircon age and Hf isotope spectra (see supplementary Table A).

U–Th–Pb data were collected on an Agilent 7700x quadrupole mass spectrometer with high purity Ar as the carrier gas (flow rate 0.98 L min^{-1}). Analyses of unknowns were bracketed with analyses of the primary zircon reference material 91500 (1062.4 ± 0.4 Ma; Wiedenbeck et al., 1995) to monitor and correct for mass fractionation and instrumental drift. A range of secondary zircon standards spanning Archean to Phanerozoic ages – R33 (419.26 ± 0.39 Ma; Black et al., 2004), GJ-1 (608.5 ± 1.5 Ma; Jackson et al., 2004) and OG1 (3465.4 ± 0.6 Ma; Stern et al., 2009) – were used to monitor data accuracy and precision, and were corrected for mass bias and fractionation based on measured

isotopic ratios of the primary reference material. During the analytical session, R33, GJ-1 and OG1 yielded weighted mean ages of 418.1 ± 2.9 (MSWD = 0.61, *n* = 20), 606.3 ± 3.7 (MSWD = 0.41, *n* = 21), 3478 ± 15 (MSWD = 0.11, *n* = 18), respectively, all of which are within 2σ of the published age (see supplementary Table B). All zircon dates older than 1.5 Ga are presented as $^{207}Pb/^{206}Pb$ ages and dates younger than 1.5 Ga are presented as $^{238}U/^{206}Pb$ ages (Spencer et al., 2016).

Lu–Hf isotopic data were collected from the same analytical volume as U–Th–Pb data on a Nu Instruments Plasma II MC-ICPMS. Measurements of ^{172}Yb, ^{173}Yb, ^{175}Lu, $^{176}Hf+Yb+Lu$, ^{177}Hf, ^{178}Hf, ^{179}Hf and ^{180}Hf were made simultaneously. Mud Tank zircon was used as the primary reference material for Hf isotope ratios, with a $^{176}Hf/^{177}Hf$ ratio of 0.282505 ± 0.000044 (Woodhead and Hergt, 2005). Corrected $^{176}Lu/^{177}Hf$ ratios were determined through processing against the R33 zircon standard (0.001989 ± 0.000869; Black et al., 2004). 91500 (0.282306 ± 0.00004; Woodhead and Hergt, 2005), FC1 (0.282172 ± 0.000042; Salters and Hart, 1991) and GJ-1 (0.282000 ± 0.000005; Morel et al., 2008) were used as secondary standards to monitor accuracy of data processing. During the analytical session, all analyzed secondary standards fell within 2σ error of reported $^{176}Hf/^{177}Hf$ values (supplementary Table B): 91500 yielded a corrected $^{176}Hf/^{177}Hf$ weighted average ratio of 0.282297 ± 0.000009 (MSWD = 0.61, *n* = 15), FC1 yielded a corrected $^{176}Hf/^{177}Hf$ weighted average ratio of 0.282146 ± 0.000010 (MSWD = 0.75, *n* = 10) and GJ-1 yielded a corrected $^{176}Hf/^{177}Hf$ weighted average ratio of 0.282001 ± 0.0000078 (MSWD = 0.99, *n* = 20). The stable $^{178}Hf/^{177}Hf$ and $^{180}Hf/^{177}Hf$ ratios for Mud Tank yielded values of 1.46712 ± 0.00001 and 1.88676 ± 0.00001, respectively. Decay constants, chondritic uniform reservoir (CHUR) and depleted mantle values are taken from Söderlund et al. (2004), Bouvier et al. (2008) and Griffin et al. (2002), respectively.

Data were reduced in Iolite (Paton et al., 2011) and in-house Excel macros. Detrital zircon data are considered concordant where the $^{207}Pb/^{206}Pb$ and $^{238}U/^{206}Pb$ systems are within 10% of age agreement. Detrital zircon population ages were assessed using Isoplot 4.15 software (Ludwig, 2012), with Excel

macros used to produce detrital zircon age probability density plots and cumulative density plots (Gehrels et al., 2008). Kernel density plots of detrital zircon age populations, and comparisons of detrital zircon age populations between samples (multidimensional scaling - MDS) were performed in the R statistical "provenance" analysis package (Vermeesch et al., 2016). MDS is based on dissimilarity measures derived from the Kolmogorov–Smirnov test, which investigates the null hypothesis that two distributions (in this case of detrital zircon population ages) are the same, and is derived from the maximum vertical distance between sample cumulative distribution curves of grain ages. Full isotopic data for the samples are given in supplementary Table A. Epsilon notation Hf isotopic data relative to CHUR at the time of crystallization [$\varepsilon Hf_{(t)}$] were computed for concordant zircon grains using the age of the crystal, and the measured (present-day) $^{176}Lu/^{177}Hf$ and $^{176}Hf/^{177}Hf$ values.

4 RESULTS OF NEW SYN-BREAKUP ZIRCON SAMPLES FROM THE PERTH BASIN

4.1 Detrital zircon textures

Transmitted and reflected light images reveal euhedral to well-rounded zircon grains in all samples (see supplemental Fig. A). Archean zircon grains are more commonly sub-angular to sub-rounded. Proterozoic and Cambrian grains are sub-angular to well-rounded but most commonly sub-rounded to well-rounded.

In CL, zircon grains exhibit cores with oscillatory, sector or patchy zoning, or are sometimes homogenous, recrystallized or metamict (Fig. 4, supplementary Fig. B). Archean grains typically show patchy or partially recrystallized oscillatory zoning (Fig. 4a, b). Paleo- and Mesoproterozoic grains predominantly exhibit oscillatory zoned or homogeneous cores (Fig. 4c–e). Neoproterozoic and Cambrian grains are predominantly patchy or sector zoned (Fig. 4f–h). Archean to Mesoproterozoic

grains occasionally show cores with zoning patterns that are truncated by rims, but these have negligible age difference from their rim (Fig. 4b). Zircon rims, where present, range from several microns to several tens of microns in thickness. Zircon rims are variably darker or lighter in CL than zircon cores for Archean to Mesoproterozoic grains, but are typically bright in Neoproterozoic grains (Fig. 4).

4.2 Detrital zircon U–Pb geochronology and Lu–Hf isotope geochemistry

Samples 7A and 7B from the basin margin exhibit unimodal detrital zircon age populations comprising >80% Neoarchean grains (peak age at ca. 2670 Ma) from both above and below Bunbury Basalt flows (Fig. 5, see Supplementary Fig. C for concordia diagrams). Sample 7A from above the Bunbury Basalt has an additional subordinate subpopulation with an age range of ca. 1300–1100 Ma (Fig. 5).

Sample BH14, within the axis of the Perth Basin, shows a polymodal detrital zircon age spectrum with a dominant 1300–1100 Ma subpopulation (peaking at ca. 1180 Ma) and minor age component peaks at ca. 2650 Ma, 1700 Ma, 900 Ma, 700 Ma and 550 Ma (Fig. 5). Where both zircon cores and thick rims were analyzed on individual grains, concordant data were the same within 2σ error; no significantly younger metamorphic overgrowths were observed (Fig. 4). However, a common phenomenon is that lighter rims – but not exceptionally bright rims – have different Hf isotopic signatures from their corresponding cores despite having dates that overlap within 2σ error (e.g., Fig. 4g).

For all new samples, Archean zircon grains record slightly positive to negative $\varepsilon Hf_{(t)}$ values, with no significant differences between the basin axis and margin samples ($\varepsilon Hf_{(t)}$ = –10 to +3, one outlier at +7; Fig 4a, b, Fig. 6). Paleoproterozoic zircon crystals have $\varepsilon Hf_{(t)}$ between –12 and –3 (Fig. 4c, Fig. 6). Mesoproterozoic (1300–1100 Ma) zircon grains exhibit a greater array of values, from more positive to highly negative εHf isotopic compositions ($\varepsilon Hf_{(t)}$ = –29 to +5, Fig. 4d, Fig. 6). Zircon

grains between 1100 and 900 Ma are predominantly chondritic ($\varepsilon Hf_{(t)}$ = –3 to +3) but some analyses have $\varepsilon Hf_{(t)}$ as low as –14 (Fig. 6). Grains dated between 750 and 650 Ma have $\varepsilon Hf_{(t)}$ around CHUR (Fig. 4f, Fig. 6). In addition to CHUR-like Hf isotopic ratios ($\varepsilon Hf_{(t)}$ = –3 to +1, one outlier at +5; Fig. 4h, Fig. 6), the 600–500 Ma zircon subpopulation has some grains with highly negative $\varepsilon Hf_{(t)}$ values between –25 and –10 (Fig. 4g, Fig. 6).

5 PRINCIPAL AGE PEAKS AND HF ISOTOPIC COMPOSITIONS IN PERTH BASIN SPECTRA LINKED TO PLAUSIBLE SOURCE TERRANES

All recognized detrital zircon age peaks have previously been linked to known source terranes, but given the shared crustal age-provinces across former Gondwanan conjugate margins and the potential for both primary vs. polycyclic sedimentary routing, significant debate remains regarding exact source region locations (Cawood and Nemchin, 2000; Cawood et al., 2003; Sircombe and Freeman, 1999; Veevers et al., 2005). Age data are complemented by published Hf (and where Hf is not available, Nd) isotopic data from key source terrains and compared to new and published detrital zircon Hf isotopic data from Permian, Triassic and Lower Cretaceous basin samples (Fig. 6).

5.1 Neoarchean (2800–2600 Ma) and older source terranes

Using both U–Pb ages and Hf isotopic signatures, Neoarchean detrital zircon grains across samples 7A, 7B, BH14 as well as the broader Perth Basin are confidently attributed to the Yilgarn Craton, which is situated along most of the eastern boundary of the Perth Basin (Figs. 3, 5, 6; Kositcin et al., 2008; Mole et al., 2013; Nemchin and Pidgeon, 1997). Older material between 3700 and 3000 Ma was also probably derived from the Yilgarn Craton (Griffin et al., 2004). Most other Archean blocks that were proximal to the Perth Basin in Gondwana lack a 2800–2600 Ma component, including the Mawson Craton and Vestfold Hills in Antarctica, and the Singhbhum Craton and Dharwar Craton in

India (Black et al., 1992; Boger, 2011; Clark et al., 2012; Jayananda et al., 2000; Jayananda et al., 2018; Mukhopadhyay et al., 2008; Sheraton et al., 1992). Only the Bunger Hills and, possibly, adjacent Obruchev Hills in Antarctica have possible 2800–2600 Ma components (Black et al., 1992; Daczko et al., 2018; Sheraton et al., 1992; Tucker et al., 2017). Tucker et al. (2017) suggested that these localities are reworked portions of the Yilgarn Craton, which would confirm that all Neoarchean material in the Perth Basin is simply derived from the Yilgarn Craton and Antarctic equivalents.

5.2 Mesoproterozoic (1300–1100 Ma) and late Paleoproterozoic (1800–1600 Ma) source terranes

Detrital zircon subpopulations defining the 1300–1100 and 1800–1600 Ma intervals in sample BH14 and, to a lesser extent, sample 7A are predominantly correlated with characteristic ages and Hf isotopic signatures of magmatism in the Albany–Fraser–Wilkes Orogen (Figs. 5, 6; Clark et al., 2000; Fitzsimons, 2000, 2003; Kirkland et al., 2011; Spaggiari et al., 2015). A small proportion of ca. 2000, 1800 and 1600 Ma detrital grains from the northern Perth Basin may have been derived from the Capricorn Orogen (Johnson et al., 2017) but at least the ca. 1800 and 1600 Ma populations are also present in the Albany–Fraser–Wilkes Orogen (Spaggiari et al., 2015). More distal blocks are unlikely to be contributors to the Perth Basin detritus; eastern Indian blocks only partially overlap in age with the Paleo- and Mesoproterozoic detritus in the Perth Basin (see references in Fig. 2).

The exact source and routing of Albany–Fraser–Wilkes Orogen detritus across the Perth Basin is controversial, with two principal models proposed: (a) first cycle – axial drainage from the south (Markwitz et al., 2017c; Sircombe and Freeman, 1999), and (b) second cycle – erosion of post-Mesoproterozoic cover on the Yilgarn Craton from the east, which was itself derived from the Albany–Fraser-Wilkes Orogen (Cawood and Nemchin, 2000; Veevers et al., 2005; Weber et al., 2005). Paleocurrent data from the northern Perth Basin reveal that drainage was predominantly northward to northwestward for all fluvial units throughout the history of the Perth Basin (Mory and

Iasky, 1996). However, paleodrainage patterns also show prominent tributaries orthogonal to the main north to northwestward drainage system that has not been sampled by paleocurrent data (Olierook et al., 2015a). Thus, paleocurrent and paleodrainage data are compatible with the majority of detritus sourced from both the south and east. Dominant Mesoproterozoic ages in detrital zircon U–Pb spectra from the Collie Basin (Fig. 5; Veevers et al., 2005) and equivalent ages in spectra from Permian paleovalleys in the eastern parts of the Yilgarn Craton (Tunmer, 2017) indicate that sedimentation on the Yilgarn Craton, at least locally in paleovalleys and the restricted Collie Basin, was occurring in the Permian, and that the cover sequence was likely derived from the Albany–Fraser–Wilkes Orogen. Apatite fission track analyses support a post-Mesoproterozoic Yilgarn Craton cover model, indicating that at least 3 km of material needed to be eroded from the northern Yilgarn Craton sometime between the Permian and Jurassic periods to account for the craton's denudation history (Kohn et al., 2002; Weber et al., 2005). A ~3 km exhumation estimate in the northern Yilgarn Craton is also similar to that calculated further south for the NW–SE Collie Basin based on its coal rank (Kohn et al., 2002; Le Blanc Smith, 1993). However, these exhumation estimates assume similar geothermal gradients to the present day and, given that heat flow is likely to have been significantly higher during rifting, they are likely to be overestimates, with a more realistic estimate of exhumation being 1–2 km (Norvick, 2003). Nevertheless, the presence of a post-Mesoproterozoic cover over the Yilgarn Craton would (a) prevent direct erosion of the Archean crystalline basement, and (b) provide a source of Proterozoic-age detritus that could have been eroded and re-deposited into the Perth Basin, thereby accounting for the limited amount of Archean material from most detrital zircon samples in the Perth Basin (Veevers et al., 2005; Weber et al., 2005). Dominance of Archean zircon grains in samples proximal to the Yilgarn Craton in both the Permian northern Perth Basin (Dillinger et al., 2018) and Cretaceous southern Perth Basin (samples 7A and B) argue against a pervasive, thick cover of Proterozoic detritus that was shedding from the east into the Perth rift basin. Furthermore, at least parts of the Yilgarn Craton must have been exposed in the Permian–Jurassic to allow for the formation of

glacigene basins and paleovalleys directly on the craton. Therefore, the presence of an extensive post-Mesoproterozoic sedimentary cover sequence on the Yilgarn Craton and the timing of its deposition remains speculative. In summary, a combination of paleocurrent data, detrital zircon U–Pb and Hf isotope spectra, and thermochronology data indicate that both axial drainage from the south and rift shoulder drainage from the east were contributors to the ca. 1800–1600 and 1300–1100 Ma detrital zircon cargo in the Perth Basin.

5.3 Late Mesoproterozoic to early Neoproterozoic (1100–900 Ma) source terranes

The ca. 1100–900 Ma detrital zircon grains are pronounced in samples in the northernmost Perth Basin, north of the E–W trending Allanooka Fault (Figs. 3, 5), and were most likely derived from the Pinjarra Orogen in Western Australia. The Pinjarra Orogen can be sampled from drill holes and outcropping inliers, namely the Leeuwin, Mullingarra and Northampton Complexes (Fig. 3; Bruguier et al., 1999; Collins, 2003; Ksienzyk et al., 2012; Markwitz et al., 2017a; Wilde, 1999). Zircon grains in the Leeuwin Complex and other Pinjarra Orogen basement in the southern Perth Basin commonly show moderate to strong Pb loss from a marked, ca. 550–500 Ma overprinting event (Arnoldi, 2017; Bodorkos et al., 2016), which is not observed in the detrital zircon from the Perth Basin. Thus, the southern parts of the Pinjarra Orogen are not considered a dominant source for the ca. 1100–900 Ma grains. The northern parts of the Pinjarra Orogen are a more suitable source for the ca. 1100–900 Ma grains in the Perth Basin because the strong ca. 550–500 Ma metamorphic overprint is not in most samples (Bodorkos et al., 2016; Bruguier et al., 1999; Cobb et al., 2001; Ksienzyk et al., 2012). A sole exception is a single drill hole (**b** in Fig. 3) along a major fault (Markwitz et al., 2017a) that was probably more prone to reactivation than any of the other sample sites in the northern parts of the Pinjarra Orogen. Furthermore, the western parts of the northern Perth Basin are also relatively shallow, implying that they could have been periodically exposed and eroded during basin fill (Olierook et al., 2015b). Finally, even though basement in the northern Pinjarra Orogen (Northampton

and Mullingarra Complexes) is dominantly paragneiss and S-type granite with only ~5–35% of zircon cores in the ca. 1100–900 Ma range, the remaining 65–95% of zircon grains are dated at ca. 1800–1600 Ma or 1300–1100 Ma grains, which match the dominant ages in most Perth Basin detrital zircon spectra (Bruguier et al., 1999; Cobb et al., 2001; Ksienzyk et al., 2012).

5.4 Neoproterozoic (750–500 Ma) source terranes

Zircon grains in sample BH14 and in other samples from the Perth Basin have bimodal Neoproterozoic age peaks at ca. 700 Ma and 550 Ma (Fig. 5), which are difficult to uniquely link to known source terranes on U–Pb age data alone. The older Neoproterozoic population from ca. 750–620 Ma is known from the Leeuwin Complex in southwest Australia (Collins, 2003; Nelson, 1996), the O'Callaghans Supersuite in the Paterson Orogen in central Australia (Czarnota et al., 2009; Haines et al., 2013) or as far away as the East African Orogen (Meert, 2003). This ca. 750–620 Ma detrital population in Perth Basin samples has $\varepsilon Hf_{(t)}$ values exclusively around the chondritic uniform reservoir (CHUR; Bouvier et al., 2008), which is similar to the available Hf and Nd data from the Leeuwin Complex (Fig. 6; Arnoldi, 2017; McCulloch, 1987). Thus, it is reasonable to attribute at least the ca. 750–620 Ma component to the Leeuwin Complex.

The younger ca. 600–500 Ma grains in Perth Basin samples could have derived from one or more of numerous terranes (Fig. 2b), including southwest Australia (Pinjarra Orogen; Bodorkos et al., 2016; Collins, 2003; Fitzsimons, 2003; Markwitz et al., 2017a; Nelson, 1996; Wilde and Murphy, 1990), East Antarctica (Prydz Bay–Denman Glacier region; Black et al., 1992; Boger, 2011; Daczko et al., 2018; Fitzsimons, 2000; Sheraton et al., 1992; Veevers and Saeed, 2011), northeastern Greater India (Shillong-Meghalaya Plateau; Chatterjee et al., 2007; Kumar et al., 2017; Yin et al., 2010) and microcontinents at what was once the Austral–Indian–Antarctic triple junction (Beslier et al., 2004; Gardner et al., 2015; Halpin et al., 2008; Halpin et al., 2017). The Leeuwin Complex has previously been cited as the principal source region for detrital zircon grains in the Perth Basin (Cawood and

Nemchin, 2000; Veevers et al., 2005). The available Hf isotopic data from the ca. 600–500 Ma age range in the Leeuwin Complex is restricted to metamorphic rims (Fig. 6; Arnoldi, 2017), and thus cannot be linked to the Perth Basin detritus. The small volume of ca. 550–500 Ma granitoid magmatism that has been identified in the Leeuwin Complex (Nelson, 1996; Wilde and Murphy, 1990) currently lacks Hf or Nd isotopic data.

Hafnium isotopic data from detrital zircon grains in the Perth Basin reveals two groups, one with $\varepsilon Hf_{(t)}$ values around CHUR and the remainder of ca. 600–500 Ma grains with evolved $\varepsilon Hf_{(t)}$ values of –10 to –30 (Fig. 6). The source of the CHUR-like detrital zircon grains may have been East Antarctica, as evidenced by similar Hf isotopic compositions from detrital zircons drained off the continent (Veevers and Saeed, 2011; Veevers et al., 2008). The source of the ca. 600–500 Ma grains with evolved $\varepsilon Hf_{(t)}$ values is most likely related to granitic plutonism associated with the Kuunga Orogeny, but the exact source is difficult to constrain. The most likely identified candidates are the Gulden Draak and Batavia Knolls, believed to have been situated close to the triple junction between India, Australia and Antarctica in Gondwana (Fig. 2; Gardner et al., 2015; Halpin et al., 2017), and the Denman Glacier region in Antarctica (Black et al., 1992; Veevers and Saeed, 2011). Granitoid samples from the two microcontinents have evolved Hf isotopic compositions ($\varepsilon Hf_{(t)}$ = –41 to –12; Gardner et al., 2015; Halpin et al., 2017), compatible with similar εHf values and oscillatory zoning found in Perth Basin samples (Fig. 6). The Denman Glacier region in Antarctica shows $\varepsilon Nd_{(t)}$ of –29 to –8 ($\varepsilon Nd_{(t)}$ calculated using ages quoted in Black et al. (1992) and, where no dates were available, an age of 550 Ma). Such low $\varepsilon Nd_{(t)}$ values are also compatible with derivation of evolved ca. 600–500 Ma zircon grains in the Perth Basin from the southwestern basement of the Pinjarra Orogen.

The Meghalaya–Shillong Plateau in northeast India also comprises granitoids of ca. 600–500 Ma age but is dominated by older basement components, primarily ca. 1800–1000 Ma in age (Fig. 2; Chatterjee et al., 2007; Kumar et al., 2017). If the Shillong–Meghalaya source was drained into the

Perth Basin, then the latter should show significant ca. 1800–1000 Ma components. Given that the ca. 1800–1600 Ma components are subordinate to the ca. 600–500 Ma grains in the Perth Basin, the Shillong–Meghalaya Plateau could not have been a dominant source (Fig. 5). Additional drill core data from the Indian and Bangladeshi basement west of the Meghalaya–Shillong Plateau is dominated by ca. 1700 Ma rocks (Ameen et al., 2007; Hossain et al., 2007; Hossain et al., 2018), which are, again, not compatible with detritus in the Perth Basin. Further north, the eastern Greater Himalayan sequence does record zircon grains with Ediacaran–Cambrian dates but these are either mixed with older detritus or too young to represent intermediate sediment reservoirs that subsequently delivered material to the Perth Basin (cf. Long and McQuarrie, 2010).

In summary, one or more of the exposed Leeuwin Complex, microcontinental fragments at the relict triple junction of eastern Gondwana, and East Antarctica may have contributed to the ca. 600–500 Ma detrital zircon subpopulation. Irrespective of whether one or a combination of these sources is responsible, it is most likely that the ca. 750–620 and ca. 600–500 Ma detrital zircon grains in the Perth Basin were derived relatively locally from the Pinjarra Orogen.

6 PROVENANCE CONTROLS IN THE PERTH BASIN

6.1 Spatial controls on provenance

6.1.1 Along-axis variation in provenance: southern vs. northern Perth Basin

There are no major systematic differences in contemporaneous detrital zircon spectra from samples collected from the southern and northern Perth Basin, implying that along-axis variation in provenance is not significant (Figs. 5, 7). There is also limited detrital zircon variation between Upper Permian–shallow marine and paralic (Kockatea Shale, Beekeeper Formation, Dongara Sandstone) and equivalent fluviatile formations (Sabina Sandstone, Wagina Sandstone; Cawood and Nemchin, 2000),

implying that depositional differences in the Perth Basin have not played a significant role in modifying the detrital zircon signature. Within the basin axis, the Mesoproterozoic Albany–Fraser–Wilkes Orogen appears to be the dominant source terrane for most samples, accounting for >50% of the detrital zircon cargo irrespective of time period and along-axis position (Figs. 5, 8, 9). The lack of along-axis variation is primarily controlled by the development of an axial drainage system that operated from south to north throughout the protracted basin history (Mory and Iasky, 1996; Olierook et al., 2015a). The axial drainage system is in turn controlled by the broadly east–west extension direction (in present-day coordinates) that was responsible for the punctuated but eventually successful breakup of eastern Gondwana (Song and Cawood, 2000; Song et al., 2001). Rifting of eastern Gondwana developed the axial drainage system that stretched from the periphery of Antarctica to the northern parts of the Perth Basin (Aitken et al., 2014; Markwitz et al., 2017c). A long (>800 km) axial drainage system is not uncommon in rift basins, particularly in association with supercontinent breakup (e.g., Rösel et al., 2014).

6.1.2 Proximity to rift axis and rift margin

The detrital zircon U–Pb age spectra of basin margin samples are markedly different to those of basin axis samples, with the former being dominated by more single-sourced Archean (Early Cretaceous, Early Permian) or Mesoproterozoic (Collie Basin) spectra (Figs. 5, 7). This indicates that detrital zircon grains in basin margin samples were derived almost exclusively from erosion of the proximal eastern rift shoulder, including some Yilgarn Craton and Albany–Fraser–Wilkes Orogen material (Fig. 7). During rifting, uplift of the basin margin may also encourage localized incision and recycling of older alluvial fans by new alluvial fans (Fig. 10), thereby diverting axial fluvial flow and yielding a stronger margin provenance signal (Gawthorpe and Leeder, 2000). These samples, deposited essentially on the rift flanks, demonstrate the significant partitioning control of rift margin faults on sediment routing systems, with a lack of material from either the basin axis or the opposite rift flank.

When comparing the detrital zircon cargo of rift shoulder samples to the basin axis sample from the Lower Permian (Cawood and Nemchin, 2000; Dillinger et al., 2018) and the Lower Cretaceous strata (this study), there is a tenfold reduction in Archean grains from margin to axis (Figs. 5, 7). This indicates that axial drainage was still dominant in the basin axis and that sediment could readily mix from axial and lateral sources. In the southern Perth Basin, the axial drainage systems during continental breakup were up to 100 km wide with many tributaries, as highlighted by aeromagnetic images of the Bunbury Basalt that has flowed into syn-breakup paleochannels (Olierook et al., 2015a). This drainage geometry is similar to present-day fluvial systems in the East African Rift Valley (Chorowicz, 2005; Rosendahl, 1987) and the Red Sea (Purser and Bosence, 2012; Younes and McClay, 2002).

6.1.3 Basin compartmentalization

The Perth Basin is strongly compartmentalized into a series of sub-basins that may have acted to guide paleodrainage and consequently influence detrital provenance (Harris, 1994; Olierook et al., 2015b; Song et al., 2001). However, variable thicknesses of specific strata in each of the sub-basins do not necessarily imply that any intrabasinal topography was present. Rather, it is possible that sediment supply kept track with the generation of accommodation space. None of the sub-basins within the basin axis show any distinct unconformities prior to continental breakup, implying that no sub-basins were topographic highs (Olierook et al., 2015b). The one exception is the Harvey Ridge, a northwest-trending sub-basin in the southern Perth Basin (Fig. 3), which shows a significant hiatus between Permian and Jurassic sedimentary rocks and may have been an intrabasinal high in the Triassic (Olierook and Timms, 2016; Olierook et al., 2015b). Apatite fission track analysis, vitrinite reflectance data and sonic transit time analysis all indicate that no exhumation occurred prior to the Cretaceous breakup in any of the basin axis sub-basins except for the Harvey Ridge (Green and Duddy, 2013; Iasky, 1993; Olierook and Timms, 2016). As indicated by these exhumation studies and

stratigraphic modelling, basement highs were probably present along the margins of the Perth Basin but these would not have affected axial drainage systems (Olierook and Timms, 2016; Song et al., 2001).

6.2 Temporal controls on provenance

6.2.1 Influence of episodes of mechanical extension vs. thermal subsidence

Independently constrained episodes of high rates of mechanical extension (rift) and lower rates of extension (thermal subsidence/post-rift) occur throughout the protracted history of the Perth Basin (Fig. 3b) and are associated with distinct provenance patterns (Fig. 5, 7). During episodes of mechanical extension, detritus from the Pinjarra Orogen (ca. 1100–500 Ma) and Yilgarn Craton (ca. 2800–2600 Ma) increase concomitantly, with broadly more Pinjarra Orogen than Yilgarn Craton material (Figs, 5, 7). The Pinjarra Orogen and Yilgarn Craton grains are present in the mid-Paleozoic Tumblagooda Sandstone (Cawood and Nemchin, 2000; Markwitz et al., 2017c), the Permian of the northern Perth Basin (Cawood and Nemchin, 2000), the Middle Triassic to Lower Jurassic in the southern Perth Basin (Lewis, 2017) and the basin axis at the time of continental breakup (BH14, this study). All these units are known to be associated with discrete rift episodes in the Perth Basin, implying that mechanical extension has controlled the input of ca. 1100–500 Ma Pinjarra Orogen and >2500 Ma Yilgarn Craton material (Fig. 3; Olierook et al., 2015b). Conversely, Pinjarra Orogen and Yilgarn Craton derived detritus is notably absent or minor in the Lower Triassic units across both the southern and northern Perth Basin (Figs. 5, 7), which are independently constrained to periods of thermal subsidence without significant mechanical extension (Olierook et al., 2015b; Song and Cawood, 2000). Thermal subsidence periods are typically characterized by a balance between the generation of long-wavelength accommodation space and sediment supply, which would promote

axial drainage rather than incorporation of material from the basin margins (Friedmann and Burbank, 1995; Gawthorpe and Leeder, 2000; Leeder and Gawthorpe, 1987).

An added degree of complexity is introduced by realizing that pure mechanical extension and thermal subsidence episodes do not exist in isolation but are only end-members to a continuum of extension rates. A pertinent example that shows this interplay between mechanical extension and thermal subsidence is the detrital zircon data from the three Lower Triassic to Lower Jurassic samples from drill hole GSWA Harvey 1 (**p** in Fig. 3) in the southern Perth Basin (Lewis, 2017; Olierook et al., 2014). GSWA Harvey 1 clearly shows an up-sequence increase of both Pinjarra Orogen (ca. 600–500 Ma) and Yilgarn Craton (ca. 2800–2600 Ma) material (Fig. 5). This is compatible with an increase of rift shoulder material with time during a transition from dominantly thermal subsidence to dominantly mechanical extension between ca. 250 to 180 Ma (Olierook et al., 2015b; Song and Cawood, 2000).

The interplay of axial and lateral (transverse) drainage during mechanical extension and thermal subsidence also provides information on the specific source of the Pinjarra Orogen material. There is a concurrence between thermal subsidence episodes and predominant Albany–Fraser–Wilkes Orogen material (Fig. 5), which indicates that the source of ca. 1300–1100 Ma grains was the primary terrane that was drained axially. It follows that the ca. 600–500 Ma Pinjarra Orogen material was a relatively minor component in axial drainage from the south or it would be present in significant quantities during thermal subsidence episodes. Therefore, the majority of ca. 600–500 Ma material was drained from the west during mechanical extension episodes, as no known source terranes with a ca. 600–500 Ma age are known from the north or east. This new interpretation indicates that detrital material was sourced from the western parts of the Pinjarra Orogen, either within the western margin of the Perth Basin or from continental fragments that were previously attached to the western margin of the West Australian Craton (Fig. 6; Bodorkos et al., 2016; Gardner et al., 2015; Halpin et al., 2017). The western parts of the Perth Basin, which include the Leeuwin Complex in the southern Perth Basin and

Turtle Dove Ridge in the northern Perth Basin, were emergent at times during basin deposition (Olierook et al., 2015b), making it entirely possible that these blocks were eroded during mechanical extension episodes.

6.2.2 Provenance after continental breakup

The Leederville Formation, deposited soon after the breakup of Australian–Antarctica and Greater India, shows a markedly different detrital U–Pb spectrum, notably a ~10:1 ratio of Archean to Neoproterozoic grains and a subordinate Mesoproterozoic peak (Figs. 5, 7). Post-breakup age spectra highlight the consequent dramatic effects on sediment supply caused by the development of oceanic crust outboard of the Perth Basin and the burial of inferred Pinjarra Orogen source to the west. Moreover, the dramatic differences in the age spectra imply that sediment recycling was secondary to primary detritus delivery. After continental breakup, the opening of the Indian Ocean and the development of the Western Australian passive margin, there was an irreversible change in drainage patterns and provenance, from axially-driven north to northwest transport direction, to topographically-driven westward transport that persists to the present day.

Modern beach sediments (e.g., Minninup Beach, Fig. 5) and Cenozoic paleocoastline sedimentary rocks along the Perth Basin passive margin show major ca. 1300–1100 Ma and ca. 750–500 Ma detrital zircon subpopulations and minor Archean input (Sircombe and Freeman, 1999). These sands are a product of: (a) recycling of older Perth Basin sedimentary rocks, with limited new input from the Yilgarn Craton, and (b) south-to-north longshore drift, with Neoproterozoic–Cambrian material derived from the Leeuwin Complex (Sircombe and Freeman, 1999; Barham, unpublished data). An important observation is that the modern day beach sands along the Western Australian coastline have the opposite proportions of 750–620 Ma and 600–500 Ma detrital zircon grains to all the pre-breakup samples (Sircombe and Freeman, 1999; Veevers et al., 2005; Barham, unpublished data). The implication is that the modern beach sands were derived from coastal erosion of the Leeuwin

Complex (with predominant ca. 750–620 Ma source rocks) but the pre-breakup samples were derived from basement blocks of the west and northwestern Pinjarra Orogen (with predominant ca. 600–500 Ma source rocks). The western and northwestern basement blocks have since either rifted away with Greater India or been buried. Further north along the modern shore, the 750–620 Ma material decreases (Sircombe and Freeman, 1999; Barham, unpublished data), further promoting the idea that the Leeuwin Complex is the only source of the Neoproterozoic ± Cambrian detritus in modern beach sands.

6.3 Primary detritus delivery vs. sediment recycling

Intrabasinal sediment recycling is often difficult to establish via detrital zircon data but there are several important sample sets in this study that argue against significant intra-rift recycling. A lack of sediment recycling is clearly demonstrated in samples from drill hole GSWA Harvey 1 (Olierook et al., 2014), which shows an up-sequence increase in Archean and Ediacaran–Cambrian detritus from the Lower Triassic Sabina Sandstone to Lower Jurassic Eneabba Formation (Figs. 5, 7; Lewis, 2017). Sediment recycling via older strata would dilute the Archean and Ediacaran–Cambrian detritus; the reality is that the opposite happened. The lack of sediment recycling is also highlighted at the basin margin, where >80% Archean grains in samples above and below the Bunbury Basalt must have been directly derived from the Yilgarn Craton. Cawood and Nemchin (2000) and Markwitz et al. (2017c) also attributed the Upper Permian and some of the mid-Paleozoic strata, respectively, to primary erosion of crystalline bedrock rather than recycling. Finally, temporal distinction of detrital zircon age spectra, and in particular, abrupt changes in sediment character post-breakup further support limited sediment recycling or homogenization. A caveat to the lack of recycling is that some sediment deposited in sub-basins adjacent to the rift margins may have been recycled into axial-draining sub-basins (Dillinger et al., 2018).

External basin recycling may have been an important control, particularly for the Albany–Fraser–Wilkes Orogen. If the notion that significant material from the Albany–Fraser–Wilkes Orogen was deposited on the Yilgarn Craton during the Paleozoic is correct, then the recycled sediment delivered to the Perth Basin may be enriched in chemically- and physically-resistant minerals, including zircon. In contrast, there is no evidence for second or later sediment delivery from the Pinjarra Orogen and Yilgarn Craton to the Perth Basin.

7 TECTONIC CONTROLS ON THE PROVENANCE EVOLUTION OF RIFT BASINS

From the spatio-temporal evaluation of provenance in the Perth Basin, there are three sediment provenance factors that are controlled by extension (Fig. 10).

First, the direction of extension defines the orientation of the basin axis and flanks as perpendicular to the extension direction. For the Perth Basin, the basin axis primarily sources detritus from the Albany–Fraser–Wilkes Orogen and the rift margin material is supplied from the Yilgarn Craton and Pinjarra Orogen (Figs. 7, 10).

Second, the ratio of rift axis to rift margin material is controlled by the rate of mechanical extension. In the Perth Basin, Ediacaran–Cambrian and Archean rift shoulders are only significant source regions for basin axis sediment during known high rates of mechanical extension (rift) events (Song and Cawood, 2000). Additionally, Paleozoic cover with ca. 1300–1100 Ma zircon grains overlying the Yilgarn Craton was also probably eroded during rifting (Veevers et al., 2005; Weber et al., 2005). During mechanical extension, the rate of subsidence is greater than sediment supply, creating positive accommodation space and creating vertical relief on rift shoulders. This then allows tributary drainage to contribute to the axial detrital zircon cargo. Importantly, the axial drainage system is still extremely effective at diluting and mixing rift shoulder detritus as evidenced from breakup-related samples,

which show an 80–100% Archean cargo on the margin to only 10% Archean in the basin axis (Fig. 5, 7). Fault block rotation at the rift margins may also be an important additional mechanism that can impede traditional marginal drainage and promote a unimodal rift margin signature (Gawthorpe and Leeder, 2000). In periods of low mechanical extension (thermal subsidence), sediment supply can buffer subsidence rates, preventing the development of scarps and minimizing input from rift shoulders.

Third, the transverse distance from the rift margin controls the efficacy of sediment mixing during episodes of mechanical extension. Published and new data show that high proportions of rift shoulder material only occur proximal to the rift margin (Figs. 3, 5, 7). Paleodrainage images from the Bunbury Basalt show that tributaries draining from the rift margin merge with the main axis on the scale of <10 km (Olierook et al., 2015a). The lack of a significant distance between the rift shoulder and basin axis explains why only samples collected very proximal (<10 km) to the basin margin show a dominant rift-shoulder signature (this study; Dillinger et al., 2018).

The proposed simple model for the tectonic control on the provenance of rift basins may be complicated by other factors, notably intrabasinal exhumation, changes in transport media (e.g., glacigene, aeolian), climate, source rock type and convergent episodes (Fig. 1). Moreover, this model also does not take into account the change in composition from source to sink, and the modification that climate and fluids have on this process. We implicitly assume that comminution and abrasion are minimal when utilizing zircon isotope systematics, but this may not necessarily be true. For example, granites with high U-bearing zircons may be more prone to metamictization and chemical alteration, which consequently reduces their ability to be transported across long distances (Markwitz et al., 2017b). Another issue that is not addressed is the homogeneity of zircon fertility of each of the basement terranes throughout their erosion and transport into the Perth Basin (Spencer et al., in press). The relative detrital contributions of the Pinjarra Orogen, Yilgarn Craton and Albany–Fraser–Wilkes

Orogen may be impacted if the zircon fertility changes stratigraphically during the progressive exhumation of each of these sources terranes. Another major caveat is that reduced erosion rates associated with arid climate conditions during deposition of the mid-Paleozoic means that comparing the Tumblagooda Sandstone with younger Permian–Cretaceous strata may have added complications that are not captured in this study. One final complexity that is difficult to test using the Perth Basin is the control of mechanical extension on the development of intrabasinal highs and subsequent influence on provenance and sediment recycling. Although the Perth Basin is now significantly exhumed, the majority of this exhumation occurred during or after continental breakup (Olierook and Timms, 2016). A notable exception is the Harvey Ridge in the southern Perth Basin (Lewis, 2017) but this does not show any systematic difference in the detrital zircon record to contemporaneous units in other parts of the basin (Fig. 5). Acknowledging these limitations, tectonic extension is probably explained by our simple three-fold model of (1) extension direction, (2) extension rates, i.e., mechanical extension vs. thermal subsidence episodes, and (3) proximity to rift margin, i.e., mixing efficacy.

8 CONCLUSIONS

Analysis of the temporal and spatial provenance evolution of the Perth Basin reveals that periods of rifting display characteristic zircon cargos throughout the protracted history of basin formation. The consistent relative proportions of principal source region detritus to the axial syn-rift sediments of the Perth Basin highlights three first order controls of extension on the provenance of a rift basin. First, the direction of extension will control the principal source terrane(s) that are drained axially through the basin. Second, the rate of mechanical extension controls the proportion of rift shoulder detritus to the basin axis, where periods with high rates of mechanical extension yield a significant proportion of rift shoulder detritus and post-rift periods of solely thermal subsidence will have negligible input of

laterally-sourced rift shoulder material. Third, during high(er) rates of mechanical extension the proximity to rift margin or rift axis will determine the relative proportions of lateral to axially-derived detritus, where samples close to the rift shoulder show only rift shoulder detritus and samples within the basin axis show mixed axial–transverse detritus.

Acknowledgements

The authors would like to thank the following: the Geological Survey of WA for their access to core; the Department of Water for their borehole logs; Andrew Economo and CMW Geosciences for donating their cores from the Bunbury Engineering project. We are also grateful to Tanya Claridge for assistance with sample preparation. GeoHistory Facility instruments in the JdLC were funded via an Australian Geophysical Observing System grant provided to AuScope Pty Ltd. by the AQ44 Australian Education Investment Fund program. The NPII multi-collector was obtained via funding from the Australian Research Council LIEF program (LE150100013). The manuscript benefited significantly from the thorough reviews of two anonymous reviewers and the editorial handling of A. S. Collins.

References

Aitken, A.R.A., Betts, P.G., Young, D.A., Blankenship, D.D., Roberts, J.L., Siegert, M.J., 2016. The Australo-Antarctic Columbia to Gondwana transition. Gondwana Research 29, 136-152.

Aitken, A.R.A., Young, D.A., Ferraccioli, F., Betts, P.G., Greenbaum, J.S., Richter, T.G., Roberts, J.L., Blankenship, D.D., Siegert, M.J., 2014. The subglacial geology of Wilkes Land, East Antarctica. Geophysical Research Letters 41, 2390-2400.

Ameen, S.M.M., Wilde, S.A., Kabir, M.Z., Akon, E., Chowdhury, K.R., Khan, M.S.H., 2007. Paleoproterozoic granitoids in the basement of Bangladesh: A piece of the Indian shield or an exotic fragment of the Gondwana jigsaw? Gondwana Research 12, 380-387.

Arnoldi, S., 2017. Spatial and temporal relationships in rocks of the Leeuwin Complex, and their setting within the Pinjarra Orogen of Western Australia, Department of Applied Geology, Honours thesis. Curtin University, Perth, WA.

Backhouse, J., 1988. Late Jurassic and Early Cretaceous palynology of the Perth Basin, Western Australia. Western Australia Geological Survey, Perth, pp. 1-233, <retrieved from http://geodocs.dmp.wa.gov.au/>.

Barham, M., Reynolds, S., Kirkland, C.L., O'Leary, M.J., Evans, N.J., Allen, H.J., Haines, P.W., Hocking, R.M., McDonald, B.J., 2018. Sediment routing and basin evolution in Proterozoic to Mesozoic east Gondwana: A case study from southern Australia. Gondwana Research 58, 122-140.

Beslier, M.O., Royer, J.Y., Girardeau, J., Hill, P.J., Boeuf, E., Buchanan, C., Chatin, F., Jacovetti, G., Moreau, A., Munschy, M., Partouche, C., Robert, U., Thomas, S., 2004. A wide ocean-continent transition along the south-west Australian margin: first results of the MARGAU/MD110 cruise. Bulletin de la Societe Géologique de France 175, 629-641.

Black, L.P., Kamo, S.L., Allen, C.M., Davis, D.W., Aleinikoff, J.N., Valley, J.W., Mundil, R., Campbell, I.H., Korsch, R.J., Williams, I.S., Foudoulis, C., 2004. Improved 206Pb/238U microprobe geochronology by the monitoring of a trace-element-related matrix effect; SHRIMP, ID–TIMS, ELA–ICP–MS and oxygen isotope documentation for a series of zircon standards. Chemical Geology 205, 115-140.

Black, L.P., Sheraton, J.W., Tingey, R.J., McCulloch, M.T., 1992. New U-Pb zircon ages from the Denman Glacier area, East Antarctica, and their significance for Gondwana reconstruction. Antarctic Science 4, 447-460.

Bodorkos, S., Fitzsimons, I.C.W., Hall, L.S., Sircombe, K.N., Lewis, C.J., 2016. Beneath the Perth Basin. New U–Pb SHRIMP zircon ages from the Pinjarra Orogen, Western Australia, 2016. Geoscience Australia Record 2016/31, p. 35.

Boger, S.D., 2011. Antarctica — Before and after Gondwana. Gondwana Research 19, 335-371.

Boger, S.D., Miller, J.M., 2004. Terminal suturing of Gondwana and the onset of the Ross–Delamerian Orogeny: the cause and effect of an Early Cambrian reconfiguration of plate motions. Earth and Planetary Science Letters 219, 35-48.

Borissova, I., Bradshaw, B.E., Nicholson, C.J., Payne, D.S., Struckmeyer, H.I.M., 2010. New exploration opportunities on the southwest Australian margin – deep-water frontier Mentelle Basin. The APPEA Journal 50, 1-13.

Boucot, A.J., Xu, C., Scotese, C.R., Morley, R.J., 2013. Phanerozoic paleoclimate: an atlas of lithologic indicators of climate. SEPM (Society for Sedimentary Geology).

Bouvier, A., Vervoort, J.D., Patchett, P.J., 2008. The Lu–Hf and Sm–Nd isotopic composition of CHUR: Constraints from unequilibrated chondrites and implications for the bulk composition of terrestrial planets. Earth and Planetary Science Letters 273, 48-57.

Bruguier, O., Bosch, D., Pidgeon, R.T., Byrne, D.I., Harris, L.B., 1999. U-Pb chronology of the Northampton Complex, Western Australia – evidence for Grenvillian sedimentation, metamorphism and deformation and geodynamic implications. Contributions to Mineralogy and Petrology 136, 258-272.

Bush, M.A., Saylor, J.E., Horton, B.K., Nie, J., 2016. Growth of the Qaidam Basin during Cenozoic exhumation in the northern Tibetan Plateau: Inferences from depositional patterns and multiproxy detrital provenance signatures. Lithosphere 8, 58-82.

Capitanio, F.A., Morra, G., Goes, S., Weinberg, R.F., Moresi, L., 2010. India-Asia convergence driven by the subduction of the Greater Indian continent. Nature Geoscience 3, 136-139.

Cawood, P.A., Hawkesworth, C., Dhuime, B., 2012. Detrital zircon record and tectonic setting. Geology 40, 875-878.

Cawood, P.A., Nemchin, A.A., 2000. Provenance record of a rift basin: U/Pb ages of detrital zircons from the Perth Basin, Western Australia. Sedimentary Geology 134, 209-234.

Cawood, P.A., Nemchin, A.A., Freeman, M., Sircombe, K., 2003. Linking source and sedimentary basin: Detrital zircon record of sediment flux along a modern river system and implications for provenance studies. Earth and Planetary Science Letters 210, 259-268.

Cawood, P.A., Wang, Y., Xu, Y., Zhao, G., 2013. Locating South China in Rodinia and Gondwana: A fragment of greater India lithosphere? Geology 41, 903-906.

Chatterjee, N., Mazumdar, A.C., Bhattacharya, A., Saikia, R.R., 2007. Mesoproterozoic granulites of the Shillong–Meghalaya Plateau: Evidence of westward continuation of the Prydz Bay Pan-African suture into Northeastern India. Precambrian Research 152, 1-26.

Chorowicz, J., 2005. The East African rift system. Journal of African Earth Sciences 43, 379-410.

Clark, C., Kinny, P.D., Harley, S.L., 2012. Sedimentary provenance and age of metamorphism of the Vestfold Hills, East Antarctica: Evidence for a piece of Chinese Antarctica? Precambrian Research 196-197, 23-45.

Clark, D.J., Hensen, B.J., Kinny, P.D., 2000. Geochronological constraints for a two-stage history of the Albany–Fraser Orogen, Western Australia. Precambrian Research 102, 155-183.

Cobb, M., Cawood, P., Kinny, P., Fitzsimons, I., 2001. SHRIMP U-Pb zircon ages from the Mullingarra Complex, Western Australia: isotopic evidence for allochthonous blocks in the Pinjarra Orogen and implications for East Gondwana assembly, Geological Society of Australia Abstracts. Geological Society of Australia; 1999, pp. 21-22.

Coffin, M.F., Pringle, M.S., Duncan, R.A., Gladczenko, T.P., Storey, M., Müller, R.D., Gahagan, L.A., 2002. Kerguelen hotspot magma output since 130 Ma. Journal of Petrology 43, 1121-1139.

Collins, A.S., 2003. Structure and age of the northern Leeuwin Complex, Western Australia: constraints from field mapping and U-Pb isotopic analysis. Australian Journal of Earth Sciences 50, 585-599.

Collins, A.S., Pisarevsky, S.A., 2005. Amalgamating eastern Gondwana: The evolution of the Circum-Indian Orogens. Earth Science Reviews 71, 229-270.

Corfu, F., Hanchar, J.M., Hoskin, P.W.O., Kinny, P., 2003. Atlas of Zircon Textures. Reviews in Mineralogy and Geochemistry 53, 469-500.

Crostella, A., Backhouse, J., 2000. Geology and petroleum exploration of the central and southern Perth Basin, Western Australia. Report 57. Geological Survey of Western Australia.

Czarnota, K., Gerner, E., Maidment, D.W., Meixner, A., Bagas, L., 2009. Paterson Area 1: 250 000 Scale Solid Geology Interpretation and Depth to Basement Model. Geoscience Australia, Canberra. Record Record 2009/16, 37.

Daczko, N.R., Halpin, J.A., Fitzsimons, I.C.W., Whittaker, J.M., 2018. A cryptic Gondwana-forming orogen located in Antarctica. Scientific Reports 8, 8371.

Dasgupta, S., Bose, S., Bhowmik, S.K., Sengupta, P., 2017. The Eastern Ghats Belt, India, in the context of supercontinent assembly. Geological Society, London, Special Publications 457, 87-104.

Dickinson, W.R., Suczek, C.A., 1979. Plate tectonics and sandstone compositions. American Association of Petroleum Geologists 63, 2164-2182.

Dillinger, A., George, A.D., Parra-Avila, L.A., 2018. Early Permian sediment provenance and paleogeographic reconstructions in southeastern Gondwana using detrital zircon geochronology (Northern Perth Basin, Western Australia). Gondwana Research 59, 57-75.

Direen, N., Cohen, B.E., Maas, R., Frey, F.A., Whittaker, J.M., Coffin, M.F., Meffre, S., Halpin, J.A., Crawford, A.J., 2017. Naturaliste Plateau: constraints on the timing and evolution of the Kerguelen Large Igneous province and its role in Gondwana breakup. Australian Journal of Earth Sciences 64, 851-869.

Eyles, N., Mory, A.J., Eyles, C.H., 2006. 50-Million-Year-Long Record of Glacial to Postglacial Marine Environments Preserved in a Carboniferous–Lower Permian Graben, Northern Perth Basin, Western Australia. Journal of Sedimentary Research 76, 618-632.

Fitzsimons, I.C.W., 2000. Grenville-age basement provinces in East Antarctica: Evidence for three separate collisional orogens. Geology 28, 879-882.

Fitzsimons, I.C.W., 2003. Proterozoic basement provinces of southern and southwestern Australia, and their correlation with Antarctica, In: Yoshida, M., Windley, B.F., Dasgupta, S. (Eds.),

Proterozoic East Gondwana: Supercontinent Assembly and Breakup. Geological Society, London, Special Publications, pp. 93-130.

Fitzsimons, I.C.W., 2016. Pan–African granulites of Madagascar and southern India: Gondwana assembly and parallels with modern Tibet. Journal of Mineralogical and Petrological Sciences 111, 73-88.

Fletcher, I.R., Libby, W.G., 1993. Further isotopic evidence for the existence of two distinct terranes in the southern Pinjarra Orogen, Western Australia. Geological Survey of Western Australia Report 37, 81-83.

Fletcher, I.R., Wilde, S.A., Rosman, K.J.R., 1985. Sm-Nd model ages across the margins of the Archaean Yilgarn Block, Western Australia — III. The western margin. Australian Journal of Earth Sciences 32, 73-82.

Friedmann, S.J., Burbank, D.W., 1995. Rift basins and supradetachment basins: Intracontinental extensional end-members. Basin Research 7, 109-127.

Gardner, R.L., Daczko, N.R., Halpin, J.A., Whittaker, J.M., 2015. Discovery of a microcontinent (Gulden Draak Knoll) offshore Western Australia: Implications for East Gondwana reconstructions. Gondwana Research 28, 1019-1031.

Gawthorpe, R., Leeder, M., 2000. Tectono-sedimentary evolution of active extensional basins. Basin Research 12, 195-218.

Gehrels, G., 2014. Detrital Zircon U-Pb Geochronology Applied to Tectonics. Annual Review of Earth and Planetary Sciences 42, 127-149.

Gehrels, G.E., Valencia, V.A., Ruiz, J., 2008. Enhanced precision, accuracy, efficiency, and spatial resolution of U-Pb ages by laser ablation–multicollector–inductively coupled plasma–mass spectrometry. Geochemistry, Geophysics, Geosystems 9, n/a-n/a.

Gibbons, A.D., Barckhausen, U., van den Bogaard, P., Hoernle, K., Werner, R., Whittaker, J.M., Müller, R.D., 2012. Constraining the Jurassic extent of Greater India: Tectonic evolution of the West Australian margin. Geochemistry, Geophysics, Geosystems 13, Q05W13.

Gibbons, A.D., Whittaker, J.M., Müller, R.D., 2013. The breakup of East Gondwana: Assimilating constraints from Cretaceous ocean basins around India into a best-fit tectonic model. Journal of Geophysical Research: Solid Earth 118, 808-822.

Glen, R.A., Fitzsimons, I.C.W., Griffin, W.L., Saeed, A., 2017. East Antarctic sources of extensive Lower–Middle Ordovician turbidites in the Lachlan Orogen, southern Tasmanides, eastern Australia. Australian Journal of Earth Sciences 64, 143-224.

Green, P.F., Duddy, I.R., 2013. The influence of exhumation on petroleum prospectivity in the sedimentary basins of WA, Western Australian Basins Symposium 2013, Perth, WA, 18-21 August 2013, pp. 1-14.

Gregory, L.C., Meert, J.G., Bingen, B., Pandit, M.K., Torsvik, T.H., 2009. Paleomagnetism and geochronology of the Malani Igneous Suite, Northwest India: Implications for the configuration of Rodinia and the assembly of Gondwana. Precambrian Research 170, 13-26.

Griffin, W.L., Belousova, E.A., Shee, S.R., Pearson, N.J., O'Reilly, S.Y., 2004. Archean crustal evolution in the northern Yilgarn Craton: U–Pb and Hf-isotope evidence from detrital zircons. Precambrian Research 131, 231-282.

Griffin, W.L., Wang, X., Jackson, S.E., Pearson, N.J., O'Reilly, S.Y., Xu, X., Zhou, X., 2002. Zircon chemistry and magma mixing, SE China: In-situ analysis of Hf isotopes, Tonglu and Pingtan igneous complexes. Lithos 61, 237-269.

Haines, P.W., Wingate, M.T.D., Kirkland, C.L., 2013. Detrital zircon U-Pb ages from the Paleozoic of the Canning and Officer basins, Western Australia: implications for provenance and interbasin connections, The Sedimentary Basins of Western Australia IV. Proceedings of the Petroleum Exploration Society of Australia Symposium, Perth, WA.

Halpin, J.A., Crawford, A.J., Direen, N.G., Coffin, M.F., Forbes, C.J., Borissova, I., 2008. Naturaliste Plateau, offshore Western Australia: a submarine window into Gondwana assembly and breakup. Geology 36, 807-810.

Halpin, J.A., Daczko, N.R., Kobler, M.E., Whittaker, J.M., 2017. Strike-slip tectonics during the Neoproterozoic–Cambrian assembly of East Gondwana: Evidence from a newly discovered microcontinent in the Indian Ocean (Batavia Knoll). Gondwana Research 51, 137-148.

Harris, L.B., 1994. Structural and Tectonic Synthesis for the Perth Basin, Western Australia. Journal of Petroleum Geology 17, 129-156.

Haughton, P.D.W., Todd, S.P., Morton, A.C., 1991. Sedimentary provenance studies. Geological Society, London, Special Publications 57, 1-11.

Hocking, R.M., 1991. The Silurian Tumblagooda Sandstone, Western Australia. Geological Survey of Western Australia, Report 27.

Horton, B.K., Anderson, V.J., Caballero, V., Saylor, J.E., Nie, J., Parra, M., Mora, A., 2015. Application of detrital zircon U-Pb geochronology to surface and subsurface correlations of

provenance, paleodrainage, and tectonics of the Middle Magdalena Valley Basin of Colombia. Geosphere 11, 1790-1811.

Hossain, I., Tsunogae, T., Rajesh, H.M., Chen, B., Arakawa, Y., 2007. Palaeoproterozoic U–Pb SHRIMP zircon age from basement rocks in Bangladesh: A possible remnant of the Columbia supercontinent. Comptes Rendus Geoscience 339, 979-986.

Hossain, I., Tsunogae, T., Tsutsumi, Y., Takahashi, K., 2018. Petrology, geochemistry and LA-ICP-MS U-Pb geochronology of Paleoproterozoic basement rocks in Bangladesh: An evaluation of calc-alkaline magmatism and implication for Columbia supercontinent amalgamation. Journal of Asian Earth Sciences 157, 22-39.

Iasky, R.P., 1993. A structural study of the southern Perth Basin, Western Australia. Geological Survey of Western Australia, Perth, pp. 1-56, <retrieved from http://geodocs.dmp.wa.gov.au/>.

Ibilola, O.O., 2017. Characterization of Early Cretaceous palynological assemblages from Bell-01 hole and the Lanco Bunbury Port Engineering holes BH01-28 (Southern Perth Basin, Western Australia. University of Western Australia, p. 33.

Jackson, S.E., Pearson, N.J., Griffin, W.L., Belousova, E.A., 2004. The application of laser ablation-inductively coupled plasma-mass spectrometry to in situ U–Pb zircon geochronology. Chemical Geology 211, 47-69.

Jayananda, M., Moyen, J.F., Martin, H., Peucat, J.J., Auvray, B., Mahabaleswar, B., 2000. Late Archaean (2550–2520 Ma) juvenile magmatism in the Eastern Dharwar craton, southern India: constraints from geochronology, Nd–Sr isotopes and whole rock geochemistry. Precambrian Research 99, 225-254.

Jayananda, M., Santosh, M., Aadhiseshan, K.R., 2018. Formation of Archean (3600–2500 Ma) continental crust in the Dharwar Craton, southern India. Earth-Science Reviews.

Johnson, S.P., Korhonen, F.J., Kirkland, C.L., Cliff, J.B., Belousova, E.A., Sheppard, S., 2017. An isotopic perspective on growth and differentiation of Proterozoic orogenic crust: From subduction magmatism to cratonization. Lithos 268–271, 76-86.

Jones, A.T., Kelman, A.P., Kennard, J.M., Le Poidevin, S., Mantle, D.J., Mory, A.J., 2012. Offshore Perth Basin Biozonation and Stratigraphy 2011, Chart 38. Geoscience Australia.

Kirkland, C.L., Smithies, R.H., Spaggiari, C.V., 2015. Foreign contemporaries – Unravelling disparate isotopic signatures from Mesoproterozoic Central and Western Australia. Precambrian Research 265, 218-231.

Kirkland, C.L., Spaggiari, C.V., Pawley, M.J., Wingate, M.T.D., Smithies, R.H., Howard, H.M., Tyler, I.M., Belousova, E.A., Poujol, M., 2011. On the edge: U–Pb, Lu–Hf, and Sm–Nd data suggests reworking of the Yilgarn craton margin during formation of the Albany-Fraser Orogen. Precambrian Research 187, 223-247.

Kohn, B.P., Gleadow, A.J.W., Brown, R.W., Gallagher, K., O'Sullivan, P.B., Foster, D.A., 2002. Shaping the Australian crust over the last 300 million years: insights from fission track thermotectonic imaging and denudation studies of key terranes. Australian Journal of Earth Sciences 49, 697-717.

Kositcin, N., Brown, S.J.A., Barley, M.E., Krapež, B., Cassidy, K.F., Champion, D.C., 2008. SHRIMP U-Pb zircon age constraints on the Late Archaean tectonostratigraphic architecture of the Eastern Goldfields Superterrane, Yilgarn Craton, Western Australia. Precambrian Research 161, 5-33.

Ksienzyk, A.K., Jacobs, J., Boger, S.D., Košler, J., Sircombe, K.N., Whitehouse, M.J., 2012. U–Pb ages of metamorphic monazite and detrital zircon from the Northampton Complex: evidence of two orogenic cycles in Western Australia. Precambrian Research 198–199, 37-50.

Kumar, S., Rino, V., Hayasaka, Y., Kimura, K., Raju, S., Terada, K., Pathak, M., 2017. Contribution of Columbia and Gondwana Supercontinent assembly- and growth-related magmatism in the evolution of the Meghalaya Plateau and the Mikir Hills, Northeast India: Constraints from U-Pb SHRIMP zircon geochronology and geochemistry. Lithos 277, 356-375.

Le Blanc Smith, G., 1993. Geology and Permian coal resources of the Collie Basin, Western Australia. Geological Survey of Western Australia Report 38.

Leeder, M., Gawthorpe, R., 1987. Sedimentary models for extensional tilt-block/half-graben basins. Geological Society, London, Special Publications 28, 139-152.

Lewis, C.J., 2017. SHRIMP U-Pb detrital zircon ages from GSWA Harvey 1, Western Australia, July 2013-June 2015. Record 2017/20. Geoscience Australia, Canberra.

Li, Z.-X., Evans, D.A.D., Halverson, G.P., 2013. Neoproterozoic glaciations in a revised global palaeogeography from the breakup of Rodinia to the assembly of Gondwanaland. Sedimentary Geology 294, 219-232.

Long, S., McQuarrie, N., 2010. Placing limits on channel flow: Insights from the Bhutan Himalaya. Earth and Planetary Science Letters 290, 375-390.

Ludwig, K., 2012. User's manual for Isoplot version 3.75–4.15: a geochronological toolkit for Microsoft. Excel Berkley Geochronological Center Special Publication.

Maritati, A., Aitken, A.R.A., Young, D.A., Roberts, J.L., Blankenship, D.D., Siegert, M.J., 2016. The tectonic development and erosion of the Knox Subglacial Sedimentary Basin, East Antarctica. Geophysical Research Letters 43, 10,728-710,737.

Markwitz, V., Kirkland, C.L., Evans, N.J., 2017a. Early Cambrian metamorphic zircon in the northern Pinjarra Orogen: Implications for the structure of the West Australian Craton margin. Lithosphere 9, 3-13.

Markwitz, V., Kirkland, C.L., Mehnert, A., Gessner, K., Shaw, J., 2017b. 3-D Characterization of Detrital Zircon Grains and its Implications for Fluvial Transport, Mixing, and Preservation Bias. Geochemistry, Geophysics, Geosystems 18, 4655-4673.

Markwitz, V., Kirkland, C.L., Wyrwoll, K.H., Hancock, E.A., Evans, N.J., Lu, Y., 2017c. Variations in Zircon Provenance Constrain Age and Geometry of an Early Paleozoic Rift in the Pinjarra Orogen, East Gondwana. Tectonics 36, 2477-2496.

Mazumder, R., De, S., Ohta, T., Flannery, D., Mallik, L., Chaudhury, T., Chatterjee, P., Ranaivoson, M.A., Arima, M., 2015. Palaeo-Mesoproterozoic sedimentation and tectonics of the Singhbhum Craton, eastern India, and implications for global and craton-specific geological events. Geological Society, London, Memoirs 43, 139-149.

McCulloch, M.T., 1987. Sm-Nd isotopic constraints on the evolution of Precambrian crust in the Australian continent. Proterozic Lithospheric Evolution, 115-130.

McLennan, S., Hemming, S., McDaniel, D., Hanson, G., 1993. Geochemical approaches to sedimentation, provenance, and tectonics. Geological Society of America Special Papers 284, 21-40.

Meert, J.G., 2003. A synopsis of events related to the assembly of eastern Gondwana. Tectonophysics 362, 1-40.

Meert, J.G., van der Voo, R., 1997. The assembly of Gondwana 800-550 Ma. Journal of Geodynamics 23, 223-235.

Meert, J.G., van der Voo, R., Ayub, S., 1995. Paleomagnetic investigation of the Neoproterozoic Gagwe lavas and Mbozi complex, Tanzania and the assembly of Gondwana. Precambrian Research 74, 225-244.

Merdith, A.S., Collins, A.S., Williams, S.E., Pisarevsky, S., Foden, J.D., Archibald, D.B., Blades, M.L., Alessio, B.L., Armistead, S., Plavsa, D., Clark, C., Müller, R.D., 2017. A full-plate global reconstruction of the Neoproterozoic. Gondwana Research 50, 84-134.

Moecher, D., Samson, S., 2006. Differential zircon fertility of source terranes and natural bias in the detrital zircon record: Implications for sedimentary provenance analysis. Earth and Planetary Science Letters 247, 252-266.

Moecher, D.P., Bowersox, J.R., Hickman, J.B., 2018. Zircon U-Pb Geochronology of Two Basement Cores (Kentucky, USA): Implications for Late Mesoproterozoic Sedimentation and Tectonics in the Eastern Midcontinent. The Journal of Geology 126, 25-39.

Mole, D.R., Fiorentini, M.L., Cassidy, K.F., Kirkland, C.L., Thebaud, N., McCuaig, T.C., Doublier, M.P., Duuring, P., Romano, S.S., Maas, R., Belousova, E.A., Barnes, S.J., Miller, J., 2013. Crustal evolution, intra-cratonic architecture and the metallogeny of an Archaean craton. Geological Society, London, Special Publications 393.

Mole, D.R., Fiorentini, M.L., Thebaud, N., Cassidy, K.F., McCuaig, T.C., Kirkland, C.L., Romano, S.S., Doublier, M.P., Belousova, E.A., Barnes, S.J., 2014. Archean komatiite volcanism

controlled by the evolution of early continents. Proceedings of the National Academy of Sciences 111, 10083-10088.

Morant, P., 1988. Donnybrook Project: Annual Report 1988. West Coast Holdings Limited, Perth, <retrieved from http://www.dmp.wa.gov.au/WAMEX-Minerals-Exploration-1476.aspx>.

Morel, M.L.A., Nebel, O., Nebel-Jacobsen, Y.J., Miller, J.S., Vroon, P.Z., 2008. Hafnium isotope characterization of the GJ-1 zircon reference material by solution and laser-ablation MC-ICPMS. Chemical Geology 255, 231-235.

Mory, A.J., Iasky, R.P., 1996. Stratigraphy and structure of the onshore northern Perth Basin, Western Australia. Western Australia Geological Survey, Perth, <retrieved from http://geodocs.dmp.wa.gov.au/>.

Mukhopadhyay, J., Beukes, N.J., Armstrong, R.A., Zimmermann, U., Ghosh, G., Medda, R.A., 2008. Dating the Oldest Greenstone in India: A 3.51-Ga Precise U-Pb SHRIMP Zircon Age for Dacitic Lava of the Southern Iron Ore Group, Singhbhum Craton. The Journal of Geology 116, 449-461.

Myers, J.S., Shaw, R.D., Tyler, I.M., 1996. Tectonic evolution of Proterozoic Australia. Tectonics 15, 1431-1446.

Nelson, D.R., 1996. Compilation of SHRIMP U-Pb zircon geochronology data, 1995. Geological Survey of Western Australia, Record 1996/5.

Nelson, D.R., 1997. Evolution of the Archaean granite-greenstone terranes of the Eastern Goldfields, Western Australia: SHRIMP U-Pb zircon constraints. Precambrian Research 83, 57-81.

Nelson, D.R., Bhattacharya, H.N., Thern, E.R., Altermann, W., 2014. Geochemical and ion-microprobe U–Pb zircon constraints on the Archaean evolution of Singhbhum Craton, eastern India. Precambrian Research 255, 412-432.

Nemchin, A.A., Pidgeon, R.T., 1997. Evolution of the Darling Range Batholith, Yilgarn Craton, Western Australia: a SHRIMP Zircon Study. Journal of Petrology 38, 625-649.

Norvick, M.S., 2003. Tectonic and stratigraphic history of the Perth Basin. Geoscience Australia, Canberra, pp. 1-30.

Olierook, H.K.H., Delle Piane, C., Timms, N.E., Esteban, L., Razaee, R., Mory, A.J., Hancock, L., 2014. Facies-based rock properties characterization for CO_2 sequestration: GSWA Harvey 1 well, Western Australia. Marine and Petroleum Geology 50, 83-102.

Olierook, H.K.H., Jourdan, F., Merle, R.E., Timms, N.E., Kusznir, N.J., Muhling, J., 2016. Bunbury Basalt: Gondwana breakup products or earliest vestiges of the Kerguelen mantle plume? Earth and Planetary Science Letters 440, 20-32.

Olierook, H.K.H., Merle, R.E., Jourdan, F., 2017. Toward a Greater Kerguelen large igneous province: Evolving mantle source contributions in and around the Indian Ocean. Lithos 282–283, 163-172.

Olierook, H.K.H., Timms, N.E., 2016. Quantifying multiple Permian–Cretaceous exhumation events during the break-up of eastern Gondwana: Sonic transit time analysis of the central and southern Perth Basin. Basin Research 28, 796-826.

Olierook, H.K.H., Timms, N.E., Merle, R.E., Jourdan, F., Wilkes, P.G., 2015a. Paleo-drainage and fault development in the southern Perth Basin, Western Australia during and after the breakup

of Gondwana from 3D modelling of the Bunbury Basalt. Australian Journal of Earth Sciences 62, 289-305.

Olierook, H.K.H., Timms, N.E., Wellmann, J.F., Corbel, S., Wilkes, P.G., 2015b. A 3D structural and stratigraphic model of the Perth Basin: Implications for sub-basin evolution. Australian Journal of Earth Sciences 62, 447-467.

Paton, C., Hellstrom, J., Paul, B., Woodhead, J., Hergt, J., 2011. Iolite: Freeware for the visualisation and processing of mass spectrometric data. Journal of Analytical Atomic Spectrometry 26, 2508-2518.

Playford, P.E., Cockbain, A.E., Low, G.H., 1976. Geology of the Perth Basin, Western Australia. Geological Survey of Western Australia, Perth, pp. 1-323, <retrieved from http://geodocs.dmp.wa.gov.au/>.

Purser, B.H., Bosence, D.W., 2012. Sedimentation and Tectonics in Rift Basins Red Sea:-Gulf of Aden. Springer Science & Business Media.

Ramm, M., 2000. Reservoir quality and its relationship to facies and provenance in Middle to Upper Jurassic sequences, northeastern North Sea. Clay Minerals 35, 77-94.

Replumaz, A., Negredo, A.M., Guillot, S., Villaseñor, A., 2010. Multiple episodes of continental subduction during India/Asia convergence: Insight from seismic tomography and tectonic reconstruction. Tectonophysics 483, 125-134.

Rösel, D., Boger, S.D., Möller, A., Gaitzsch, B., Barth, M., Oalmann, J., Zack, T., 2014. Indo-Antarctic derived detritus on the northern margin of Gondwana: evidence for continental-scale sediment transport. Terra Nova 26, 64-71.

Rosendahl, B.R., 1987. Architecture of continental rifts with special reference to East Africa. Annual Review of Earth and Planetary Sciences 15, 445-503.

Salters, V.J.M., Hart, S.R., 1991. The mantle sources of ocean ridges, islands and arcs: the Hf-isotope connection. Earth and Planetary Science Letters 104, 364-380.

Sanyal, S., Sengupta, P., 2012. Metamorphic evolution of the Chotanagpur Granite Gneiss Complex of the East Indian Shield: current status. Geological Society, London, Special Publications 365, 117-145.

Schmitt, R.d.S., Fragoso, R.d.A., Collins, A.S., 2018. Suturing Gondwana in the Cambrian: The Orogenic Events of the Final Amalgamation, In: Siegesmund, S., Basei, M.A.S., Oyhantçabal, P., Oriolo, S. (Eds.), Geology of Southwest Gondwana. Springer International Publishing, Cham, pp. 411-432.

Scotese, C.R., Boucot, A.J., Chen, X., 2014. Atlas of Phanerozoic Climatic Zones (Mollweide Projection), Volumes 1-6, PALEOMAP Project PaleoAtlas for ArcGIS, PALEOMAP Project, Evanston, Illinois.

Shao, L., Cao, L., Pang, X., Jiang, T., Qiao, P., Zhao, M., 2016. Detrital zircon provenance of the Paleogene syn-rift sediments in the northern South China Sea. Geochemistry, Geophysics, Geosystems 17, 255-269.

Sheraton, J.W., Black, L.P., Tindle, A.G., 1992. Petrogenesis of plutonic rocks in a Proterozoic granulite-facies terrane — the Bunger Hills, East Antarctica. Chemical Geology 97, 163-198.

Shi, Y., Hou, C., Anderson, J.L., Yang, T., Ma, Y., Bian, W., Jin, J., 2018. Zircon SHRIMP U–Pb age of Late Jurassic OIB-type volcanic rocks from the Tethyan Himalaya: constraints on the initial activity time of the Kerguelen mantle plume. Acta Geochimica 37, 441-455.

Sircombe, K.N., Freeman, M.J., 1999. Provenance of detrital zircons on the Western Australia coastline—Implications for the geologic history of the Perth basin and denudation of the Yilgarn craton. Geology 27, 879-882.

Söderlund, U., Patchett, P.J., Vervoort, J.D., Isachsen, C.E., 2004. The 176Lu decay constant determined by Lu–Hf and U–Pb isotope systematics of Precambrian mafic intrusions. Earth and Planetary Science Letters 219, 311-324.

Song, T., Cawood, P.A., 2000. Structural styles in the Perth Basin associated with the Mesozoic break-up of Greater India and Australia. Tectonophysics 317, 55-72.

Song, T., Cawood, P.A., Middleton, M., 2001. Transfer zones normal and oblique to rift trend: examples from the Perth Basin, Western Australia. Geological Society, London, Special Publications 187, 475-488.

Spaggiari, C.V., Kirkland, C.L., Smithies, R.H., Wingate, M.T.D., Belousova, E.A., 2015. Transformation of an Archean craton margin during Proterozoic basin formation and magmatism: The Albany–Fraser Orogen, Western Australia. Precambrian Research 266, 440-466.

Spencer, C.J., Cavosie, A.J., Raub, T.D., Rollinson, H., Jeon, H., Searle, M.P., Miller, J.A., McDonald, B.J., Evans, N.J., 2017. Evidence for melting mud in Earth's mantle from extreme oxygen isotope signatures in zircon. Geology 45, 975-978.

Spencer, C.J., Kirkland, C.L., Roberts, N.M.W., in press. Implications of erosion and bedrock composition on zircon fertility: Examples from South America and Western Australia. Terra Nova.

Spencer, C.J., Kirkland, C.L., Taylor, R.J.M., 2016. Strategies towards statistically robust interpretations of in situ U–Pb zircon geochronology. Geoscience Frontiers 7, 581-589.

Stern, R.A., Bodorkos, S., Kamo, S.L., Hickman, A.H., Corfu, F., 2009. Measurement of SIMS Instrumental Mass Fractionation of Pb Isotopes During Zircon Dating. Geostandards and Geoanalytical Research 33, 145-168.

Torsvik, T.H., Carter, L.M., Ashwal, L.D., Bhushan, S.K., Pandit, M.K., Jamtveit, B., 2001. Rodinia refined or obscured: palaeomagnetism of the Malani igneous suite (NW India). Precambrian Research 108, 319-333.

Tucker, N.M., Payne, J.L., Clark, C., Hand, M., Taylor, R.J.M., Kylander-Clark, A.R.C., Martin, L., 2017. Proterozoic reworking of Archean (Yilgarn) basement in the Bunger Hills, East Antarctica. Precambrian Research 298, 16-38.

Tunmer, W., 2017. Nature and distribution of residual and transported cover in the Southern Yamarna Belt, WA, Department of Applied Geology. Curtin University, p. 55.

Veevers, J.J., Saeed, A., 2011. Age and composition of Antarctic bedrock reflected by detrital zircons, erratics, and recycled microfossils in the Prydz Bay–Wilkes Land–Ross Sea–Marie Byrd Land sector (70°–240°E). Gondwana Research 20, 710-738.

Veevers, J.J., Saeed, A., Belousova, E.A., Griffin, W.L., 2005. U–Pb ages and source composition by Hf-isotope and trace-element analysis of detrital zircons in Permian sandstone and modern sand from southwestern Australia and a review of the paleogeographical and denudational history of the Yilgarn Craton. Earth-Science Reviews 68, 245-279.

Veevers, J.J., Saeed, A., O'Brien, P.E., 2008. Provenance of the Gamburtsev Subglacial Mountains from U–Pb and Hf analysis of detrital zircons in Cretaceous to Quaternary sediments in Prydz Bay and beneath the Amery Ice Shelf. Sedimentary Geology 211, 12-32.

Vermeesch, P., 2004. How many grains are needed for a provenance study? Earth and Planetary Science Letters 224, 441-451.

Vermeesch, P., Resentini, A., Garzanti, E., 2016. An R package for statistical provenance analysis. Sedimentary Geology 336, 14-25.

Vincent, S.J., Morton, A.C., Hyden, F., Fanning, M., 2013. Insights from petrography, mineralogy and U–Pb zircon geochronology into the provenance and reservoir potential of Cenozoic siliciclastic depositional systems supplying the northern margin of the Eastern Black Sea. Marine and Petroleum Geology 45, 331-348.

Weber, U.D., Kohn, B.P., Gleadow, A.J.W., Nelson, D.R., 2005. Low temperature Phanerozoic history of the Northern Yilgarn Craton, Western Australia. Tectonophysics 400, 127-151.

Weltje, G.J., von Eynatten, H., 2004. Quantitative provenance analysis of sediments: review and outlook. Sedimentary Geology 171, 1-11.

Wiedenbeck, M., AllÉ, P., Corfu, F., Griffin, W.L., Meier, M., Oberli, F., Quadt, A.V., Roddick, J.C., Spiegel, W., 1995. Three natural zircon standards For U-Th-Pb, Lu-Hf, trace element And REE analyses. Geostandards Newsletter 19, 1-23.

Wilde, S., Walker, I., 1977. Palaeocurrent directions in the Permian Collie Coal Measures, Collie, Western Australia. West. Aust. Geol. Surv. Annu. Rep, 41-43.

Wilde, S.A., 1999. Evolution of the Western Margin of Australia during the Rodinian and Gondwanan Supercontinent Cycles. Gondwana Research 2, 481-499.

Wilde, S.A., Murphy, D.M.K., 1990. The nature and origin of Late Proterozoic high-grade gneisses of the Leeuwin Block, Western Australia. Precambrian Research 47, 251-270.

Williams, S.E., Whittaker, J.M., Müller, R.D., 2011. Full-fit, palinspastic reconstruction of the conjugate Australian-Antarctic margins. Tectonics 30.

Wingate, M.T.D., Giddings, J.W., 2000. Age and palaeomagnetism of the Mundine Well dyke swarm, Western Australia: implications for an Australia–Laurentia connection at 755 Ma. Precambrian Research 100, 335-357.

Woodhead, J.D., Hergt, J.M., 2005. A Preliminary Appraisal of Seven Natural Zircon Reference Materials for In Situ Hf Isotope Determination. Geostandards and Geoanalytical Research 29, 183-195.

Yang, J., Xu, Z., Dobrzhinetskaya, L.F., Green, H.W., Pei, X., Shi, R., Wu, C., Wooden, J.L., Zhang, J., Wan, Y., Li, H., 2003. Discovery of metamorphic diamonds in central China: an indication of a >4000-km-long zone of deep subduction resulting from multiple continental collisions. Terra Nova 15, 370-379.

Yin, A., Dubey, C., Webb, A., Kelty, T., Grove, M., Gehrels, G., Burgess, W., 2010. Geologic correlation of the Himalayan orogen and Indian craton: Part 1. Structural geology, U-Pb zircon geochronology, and tectonic evolution of the Shillong Plateau and its neighboring regions in NE India. Bulletin 122, 336-359.

Younes, A.I., McClay, K., 2002. Development of accommodation zones in the Gulf of Suez-Red Sea rift, Egypt. AAPG Bulletin 86, 1003-1026.

Figure captions

Fig. 1: Controls and processes that influence the ability to reconstruct provenance from a basin fill. Tectonics and climate are the overall controls that govern various factors and key processes involved in cycling source material into a final sedimentary rock.

Fig. 2: Plate reconstruction of (a) Gondwana and (b) eastern Gondwana (modified from Aitken et al., 2014; Daczko et al., 2018; Fitzsimons, 2016; Halpin et al., 2017; Williams et al., 2011). Note that the microcontinents at the triple junction are placed so that the Naturaliste Plateau is unmoved from its present day position in line with interpretations that the basin between mainland Australia and the Naturaliste Plateau is a failed rift (Borissova et al., 2010; Direen et al., 2017; Olierook et al., 2017). CGGC = Chotanagpur Granite Gneiss Complex (Sanyal and Sengupta, 2012), EGP = Eastern Ghats Province (Dasgupta et al., 2017), M = Maddhapara granitoid (Hossain et al., 2018), SC = Singhbhum Craton and supracrustal province (Mazumder et al., 2015; Nelson et al., 2014).

Fig. 3: (a) Map of the Perth Basin showing depth to basement after Olierook et al. (2015b). AF = Allanooka Fault, AFWO = Albany–Fraser–Wilkes Orogen, LC = Leeuwin Complex, MI = Mullingarra Inlier, NC = Northampton Complex. (b) Schematic stratigraphic column after Olierook et al. (2015b) and rift phases modified from Hocking (1991) and Song and Cawood (2000). Lettering in coloured circles on the map correspond to equivalent symbols in the stratigraphic column. Sample locations in the stratigraphic column are approximate only. Note that one sample location from Cawood and Nemchin (2000) and seven from Markwitz et al. (2017c) in the mid-Paleozoic Tumblagooda Sandstone immediately north of the Northampton Complex and one Permian sample

from the Collie Basin (Veevers et al., 2005) are omitted for clarity. Published detrital zircon U–Pb data from the Perth Basin are from Sircombe and Freeman (1999), Cawood and Nemchin (2000), Markwitz et al. (2017c), Lewis (2017) and Dillinger et al. (2018). Unpublished data from the Jurassic Yarragadee Formation are from Baddock (2018, writ. comms.).

Fig. 4: Representative cathodoluminescence (CL) images of detrital zircon grains from the newly analyzed samples in the Perth Basin. Circles correspond to analytical spot locations. A compilation of all CL images with annotated age data may be found in Supplementary Figure B. Dates are calculated from $^{207}Pb/^{206}Pb$ ratios when older than 1.5 Ga and $^{206}Pb/^{238}U$ for <1.5 Ga. All dates and $\varepsilon Hf_{(t)}$ uncertainties are labelled at 2σ confidence.

Fig. 5: Probability density estimate (black lines) and kernel density estimation (red line) of detrital zircon age populations within the Perth Basin from approximately oldest sample set at the bottom to youngest sample set at the top. Grey filled spectra are from this study. All plotted zircon data is <10% discordant. n = the number of zircon grains represented, with the number of concordant analyses to total numbers of analyses provided for samples 7A, 7B and BH14. Fm. = Formation; Gp. = Group; L. = Lower; NPB = Northern Perth Basin; SPB = Southern Perth Basin; Sst. = Sandstone; U. = Upper. Vertical colored bars in the background correspond to likely source regions: PO = Pinjarra Orogen (Black et al., 1992; Collins, 2003; Gardner et al., 2015; Halpin et al., 2017; Ksienzyk et al., 2012); LC = Leeuwin Complex, the southwestern portion of the Pinjarra Orogen (Collins, 2003; Nelson, 1996); AFW = Albany–Fraser–Wilkes Orogen (Kirkland et al., 2015; Kirkland et al., 2011); YC = Yilgarn Craton (Nelson, 1997; Veevers et al., 2005).

Fig. 6: Hf isotope data for the Perth Basin and postulated basement provinces for dates with <10 % discordance. Detrital zircon data from this study, Cawood and Nemchin (2000) and Veevers et al. (2005). Source terranes include the Yilgarn Craton (Mole et al., 2014), Albany–Fraser–Wilkes Orogen (Kirkland et al., 2015), Leeuwin Complex (Arnoldi, 2017) and Batavia & Gulden Draak Knolls (Gardner et al., 2015; Halpin et al., 2017). CHUR = Chondritic uniform reservoir (Bouvier et al., 2008).

Fig. 7: Ternary plot showing relative contributions normalized to the Pinjarra Orogen (1100–500 Ma), Albany–Fraser–Wilkes Orogen (1800–1100 Ma) and Yilgarn Craton (>2500 Ma) for Perth Basin detrital zircon age spectra. Dark grey and light grey fields group rift axis samples from rift and post-rift phases, respectively.

Fig. 8: Cumulative probability plot of detrital zircon age populations from samples in the Perth Basin from Figure 5. Vertical colored bars are indicative of the ages of characteristic rock-forming events in a particular crustal region and indicate sourcing of materials where a coincident inflection occurs in the cumulative probability function. See Figure 5 for explanation of abbreviations and references for data sources.

Fig. 9: Multi-dimensional scaling plot developed from cumulative probability plots in Figure 8. Greater distance between points reflects more different detrital zircon age spectra. Vectors indicate the key ages that are causing dispersion of the data. Notice the similarities of the mechanical-rift phase associated sediments in the basin axis (cf. Fig. 7). Sample prefixes indicate the basin position

and depositional age of the sediment – NPB = northern Perth Basin; SPB = southern Perth Basin, Cret. = Cretaceous; Tri. = Triassic; L. Perm. = Lower Permian; U. Perm. = Upper Permian.

Fig. 10: Schematic diagram showing the relative contributions between axially-derived and rift shoulder-derived detritus, modified from Leeder and Gawthorpe (1987). Terranes, faults and north arrow are for the Perth Basin specifically but this model can be applicable to other rift basins.

Table 1: Location of newly-collected samples from drill cores. Flow context from Olierook et al. (2015a). Mbsl = meters below sea level; Pv. = Paleovalley

Table 1

Sample no.	Coordinates[a] Latitude	Longitude	Drill Hole	Flow context	Unit	Depth (mbsl) Start	End
7A	-33.593	115.816	Donnybrook DDB7	Donnybrook Pv., above flows	Parmelia Group	41.4	41.9
BH14	-33.312	115.669	Bunbury Port Hole 14	Bunbury Pv., between flows	Parmelia Group	31.7	32.1
7B	-33.593	115.816	Donnybrook DDB7	Donnybrook Pv., below flows	Parmelia Group	108.3	108.8

[a]All coordinates used GCS WGS84

Highlights

- Detrital zircon U–Pb and Hf isotopic data compiled for Perth Basin
- New zircon data across Gondwana breakup unconformity mostly from Archean Yilgarn Craton
- Sedimentary provenance controlled by extension direction, extension rate and distance to margin
- Three-fold tectonic control model applicable to other rift basins with minimal intrabasinal recycling

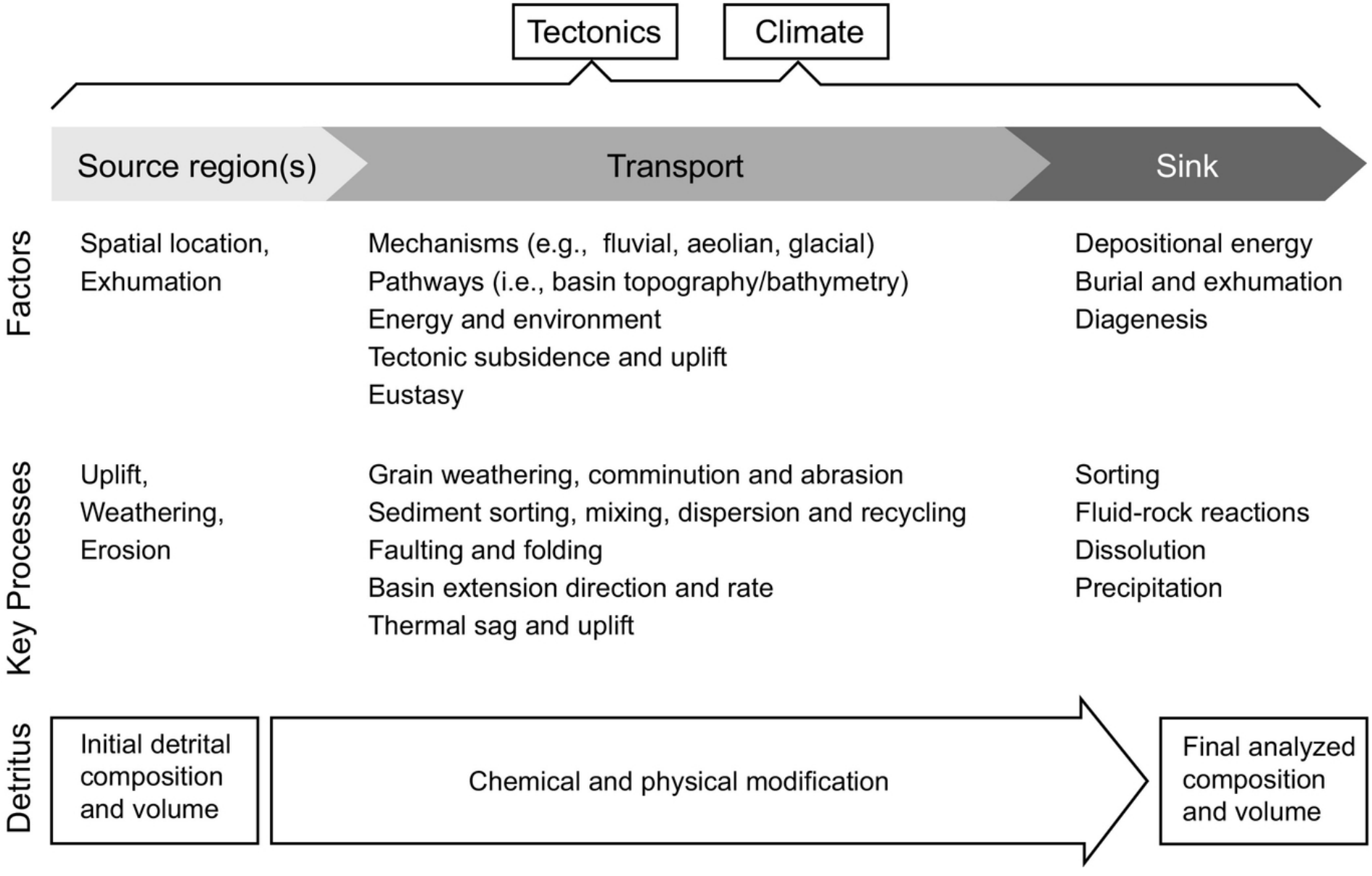
Tectonics
Climate
Source region(s)
Transport
Sink
Factors
Spatial location,
Exhumation
Mechanisms (e.g., fluvial, aeolian, glacial)
Pathways (i.e., basin topography/bathymetry)
Energy and environment
Tectonic subsidence and uplift
Eustasy
Depositional energy
Burial and exhumation
Diagenesis
Key Processes
Uplift,
Weathering,
Erosion
Grain weathering, comminution and abrasion
Sediment sorting, mixing, dispersion and recycling
Faulting and folding
Basin extension direction and rate
Thermal sag and uplift
Sorting
Fluid-rock reactions
Dissolution
Precipitation
Detritus
Initial detrital composition and volume
Chemical and physical modification
Final analyzed composition and volume

Figure 1

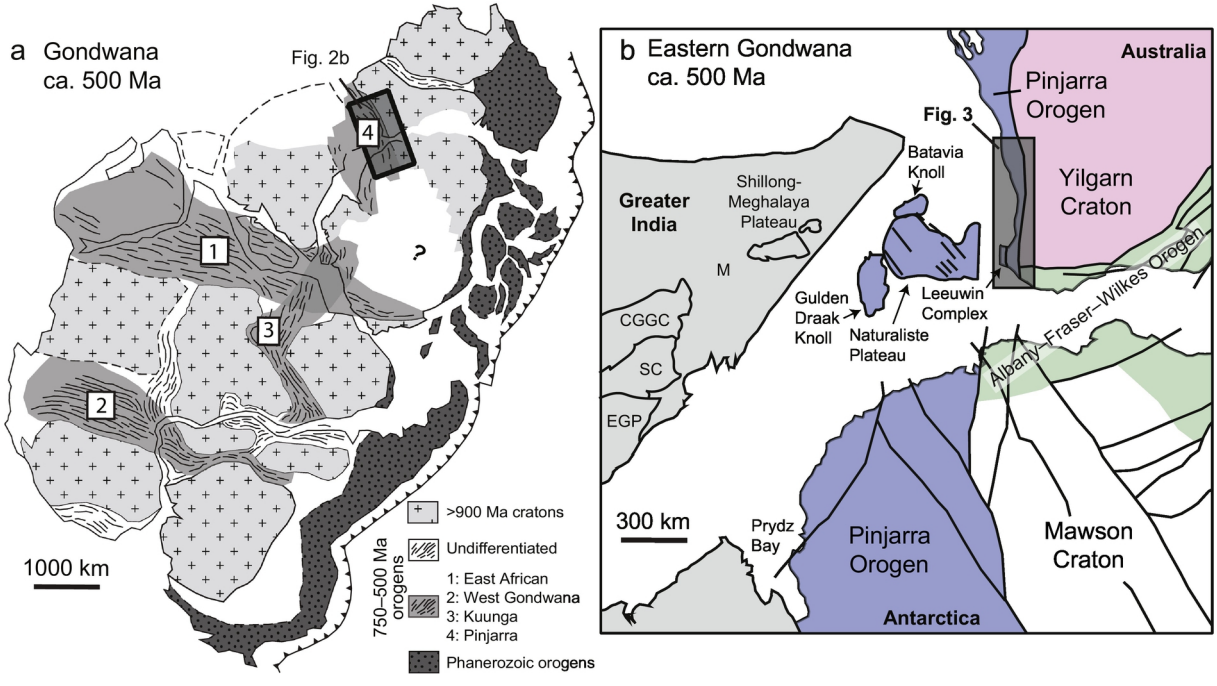
a Gondwana
ca. 500 Ma
Fig. 2b
4
1
2
3
?
1000 km
>900 Ma cratons
Undifferentiated
750–500 Ma orogens
1: East African
2: West Gondwana
3: Kuunga
4: Pinjarra
Phanerozoic orogens
b Eastern Gondwana
ca. 500 Ma
Australia
Pinjarra Orogen
Fig. 3
Batavia Knoll
Yilgarn Craton
Greater India
Shillong-Meghalaya Plateau
M
CGGC
SC
EGP
Gulden Draak Knoll
Naturaliste Plateau
Leeuwin Complex
Albany–Fraser–Wilkes Orogen
300 km
Prydz Bay
Pinjarra Orogen
Mawson Craton
Antarctica

Figure 2

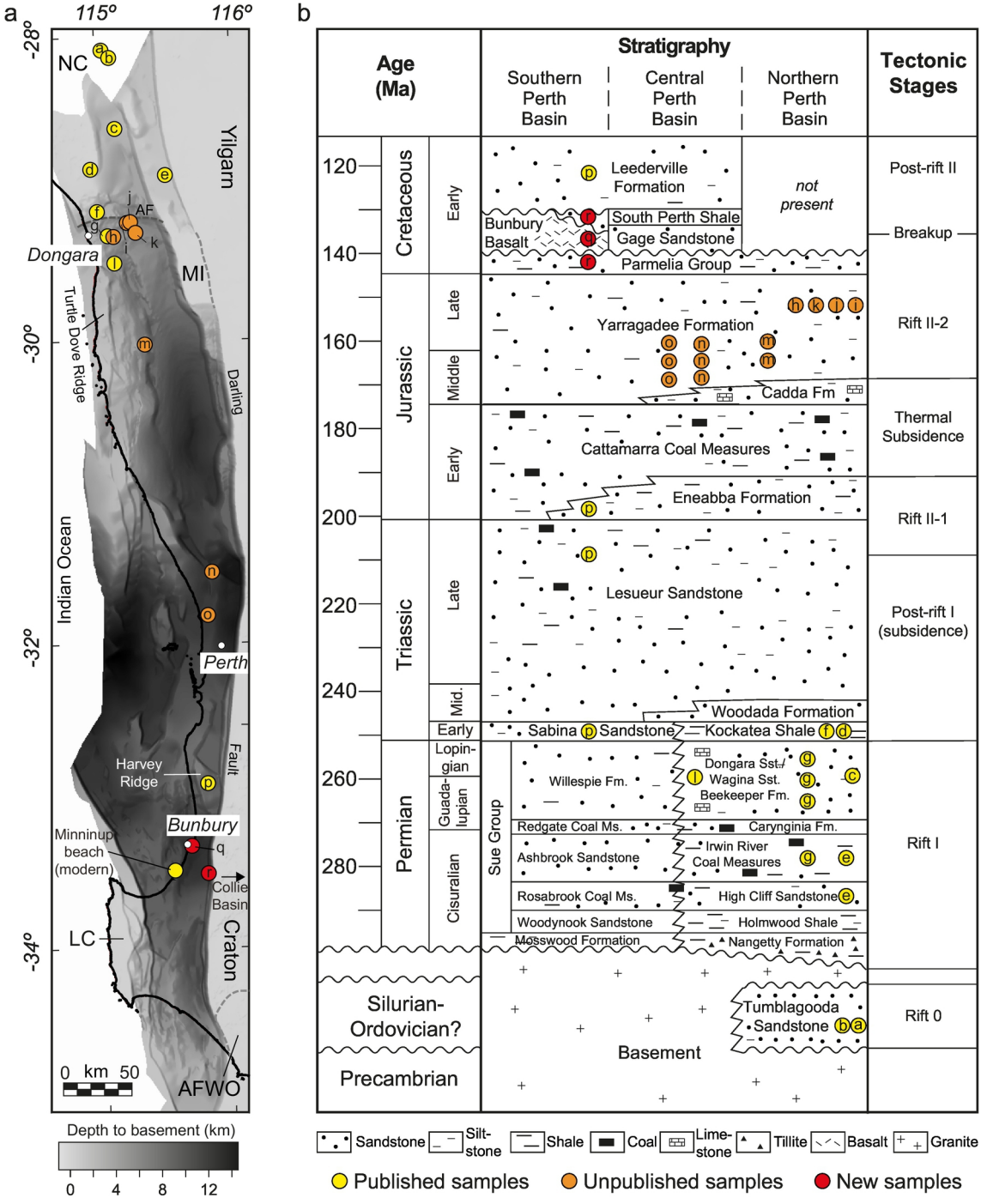
a
115°
116°
-28°
-30°
-32°
-34°
NC
Yilgarn
Dongara
MI
AF
Turtle Dove Ridge
Darling
Indian Ocean
Perth
Harvey Ridge
Fault
Bunbury
Minninup beach (modern)
Collie Basin
LC
Craton
AFWO
0 km 50
Depth to basement (km)
0
4
8
12
b
Age (Ma)
Stratigraphy
Southern Perth Basin
Central Perth Basin
Northern Perth Basin
Tectonic Stages
120
140
160
180
200
220
240
260
280
Cretaceous
Early
Jurassic
Late
Middle
Early
Triassic
Late
Mid.
Early
Permian
Lopingian
Guadalupian
Cisuralian
Leederville Formation
not present
Bunbury Basalt
South Perth Shale
Gage Sandstone
Parmelia Group
Yarragadee Formation
Cadda Fm
Cattamarra Coal Measures
Eneabba Formation
Lesueur Sandstone
Woodada Formation
Sabina Sandstone
Kockatea Shale
Sue Group
Willespie Fm.
Dongara Sst./ Wagina Sst.
Beekeeper Fm.
Redgate Coal Ms.
Caryngina Fm.
Ashbrook Sandstone
Irwin River Coal Measures
Rosabrook Coal Ms.
High Cliff Sandstone
Woodynook Sandstone
Holmwood Shale
Mosswood Formation
Nangetty Formation
Silurian-Ordovician?
Tumblagooda Sandstone
Basement
Precambrian
Post-rift II
Breakup
Rift II-2
Thermal Subsidence
Rift II-1
Post-rift I (subsidence)
Rift I
Rift 0
Sandstone
Silt-stone
Shale
Coal
Lime-stone
Tillite
Basalt
Granite
Published samples
Unpublished samples
New samples

Figure 3

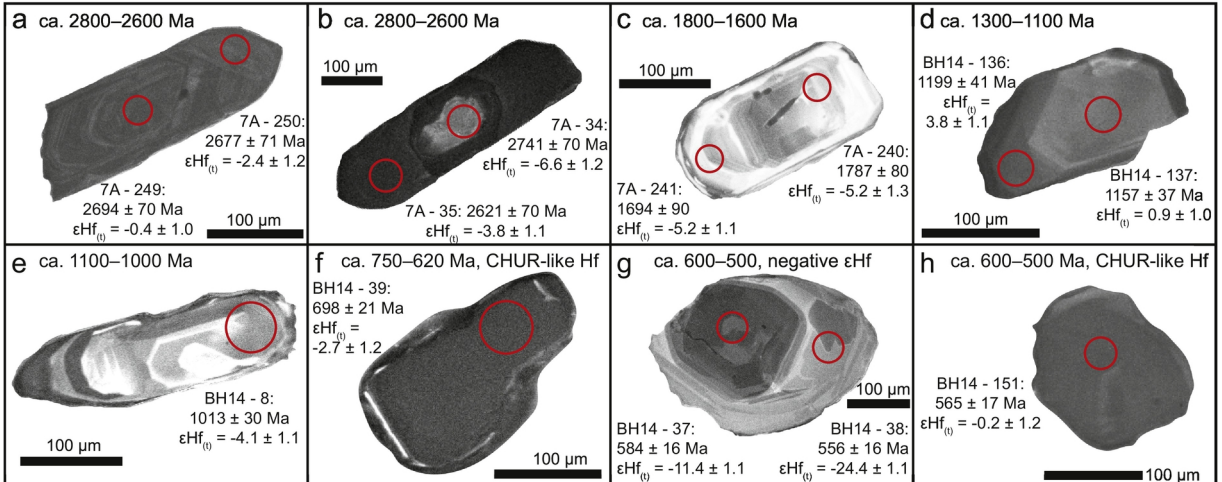
a ca. 2800–2600 Ma
7A - 250:
2677 ± 71 Ma
εHf(t) = -2.4 ± 1.2
7A - 249:
2694 ± 70 Ma
εHf(t) = -0.4 ± 1.0
100 µm
b ca. 2800–2600 Ma
100 µm
7A - 34:
2741 ± 70 Ma
εHf(t) = -6.6 ± 1.2
7A - 35: 2621 ± 70 Ma
εHf(t) = -3.8 ± 1.1
c ca. 1800–1600 Ma
100 µm
7A - 240:
1787 ± 80
εHf(t) = -5.2 ± 1.3
7A - 241:
1694 ± 90
εHf(t) = -5.2 ± 1.1
d ca. 1300–1100 Ma
BH14 - 136:
1199 ± 41 Ma
εHf(t) =
3.8 ± 1.1
BH14 - 137:
1157 ± 37 Ma
εHf(t) = 0.9 ± 1.0
100 µm
e ca. 1100–1000 Ma
BH14 - 8:
1013 ± 30 Ma
εHf(t) = -4.1 ± 1.1
100 µm
f ca. 750–620 Ma, CHUR-like Hf
BH14 - 39:
698 ± 21 Ma
εHf(t) =
-2.7 ± 1.2
100 µm
g ca. 600–500, negative εHf
100 µm
BH14 - 37:
584 ± 16 Ma
εHf(t) = -11.4 ± 1.1
BH14 - 38:
556 ± 16 Ma
εHf(t) = -24.4 ± 1.1
h ca. 600–500 Ma, CHUR-like Hf
BH14 - 151:
565 ± 17 Ma
εHf(t) = -0.2 ± 1.2
100 µm

Figure 4

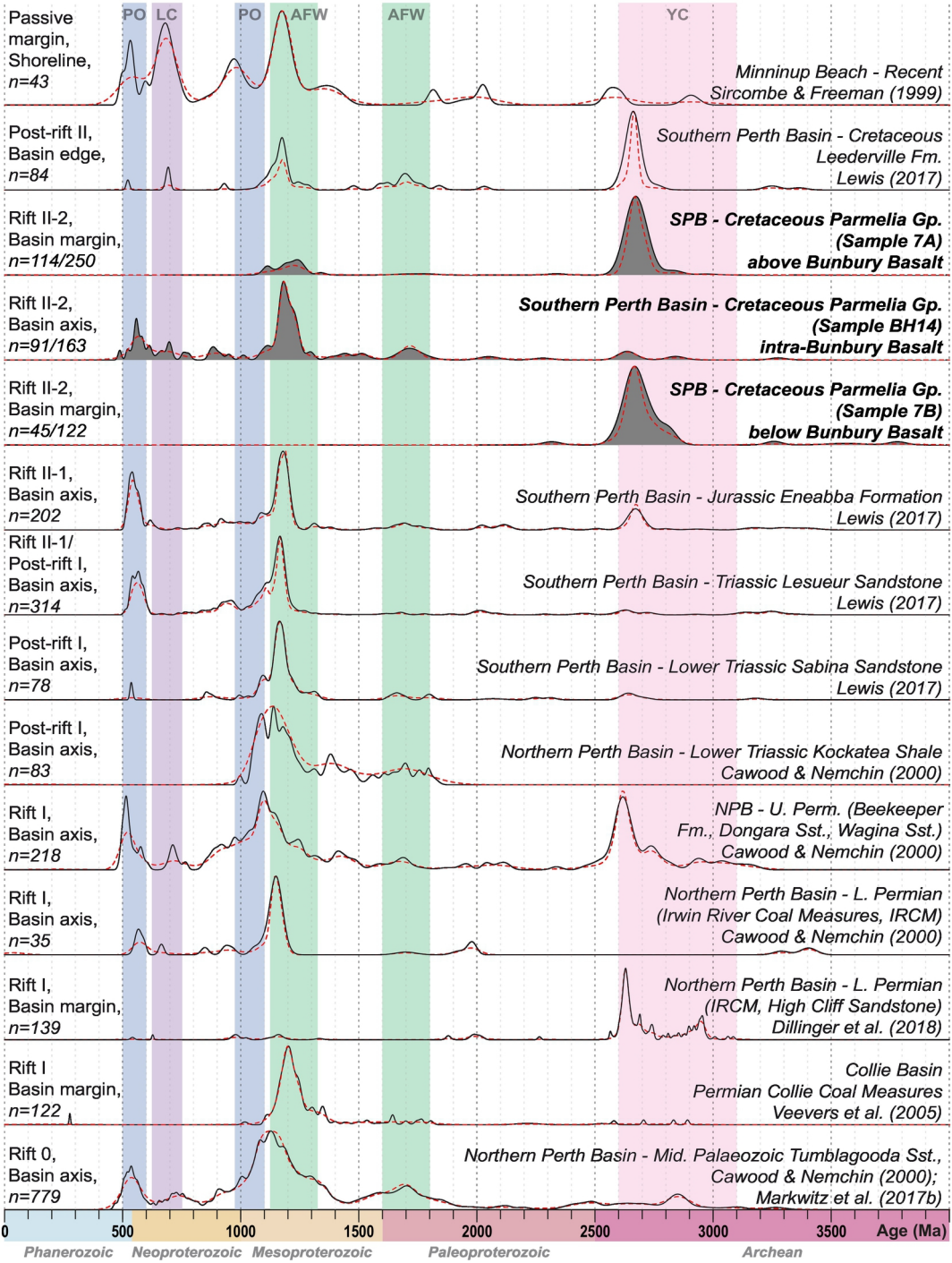
PO
LC
PO
AFW
AFW
YC
Passive margin, Shoreline, n=43
Minninup Beach - Recent
Sircombe & Freeman (1999)
Post-rift II, Basin edge, n=84
Southern Perth Basin - Cretaceous
Leederville Fm.
Lewis (2017)
Rift II-2, Basin margin, n=114/250
SPB - Cretaceous Parmelia Gp.
(Sample 7A)
above Bunbury Basalt
Rift II-2, Basin axis, n=91/163
Southern Perth Basin - Cretaceous Parmelia Gp.
(Sample BH14)
intra-Bunbury Basalt
Rift II-2, Basin margin, n=45/122
SPB - Cretaceous Parmelia Gp.
(Sample 7B)
below Bunbury Basalt
Rift II-1, Basin axis, n=202
Southern Perth Basin - Jurassic Eneabba Formation
Lewis (2017)
Rift II-1/ Post-rift I, Basin axis, n=314
Southern Perth Basin - Triassic Lesueur Sandstone
Lewis (2017)
Post-rift I, Basin axis, n=78
Southern Perth Basin - Lower Triassic Sabina Sandstone
Lewis (2017)
Post-rift I, Basin axis, n=83
Northern Perth Basin - Lower Triassic Kockatea Shale
Cawood & Nemchin (2000)
Rift I, Basin axis, n=218
NPB - U. Perm. (Beekeeper
Fm., Dongara Sst., Wagina Sst.)
Cawood & Nemchin (2000)
Rift I, Basin axis, n=35
Northern Perth Basin - L. Permian
(Irwin River Coal Measures, IRCM)
Cawood & Nemchin (2000)
Rift I, Basin margin, n=139
Northern Perth Basin - L. Permian
(IRCM, High Cliff Sandstone)
Dillinger et al. (2018)
Rift I Basin margin, n=122
Collie Basin
Permian Collie Coal Measures
Veevers et al. (2005)
Rift 0, Basin axis, n=779
Northern Perth Basin - Mid. Palaeozoic Tumblagooda Sst.,
Cawood & Nemchin (2000);
Markwitz et al. (2017b)
0
500
1000
1500
2000
2500
3000
3500
Age (Ma)
Phanerozoic
Neoproterozoic
Mesoproterozoic
Paleoproterozoic
Archean

Figure 5

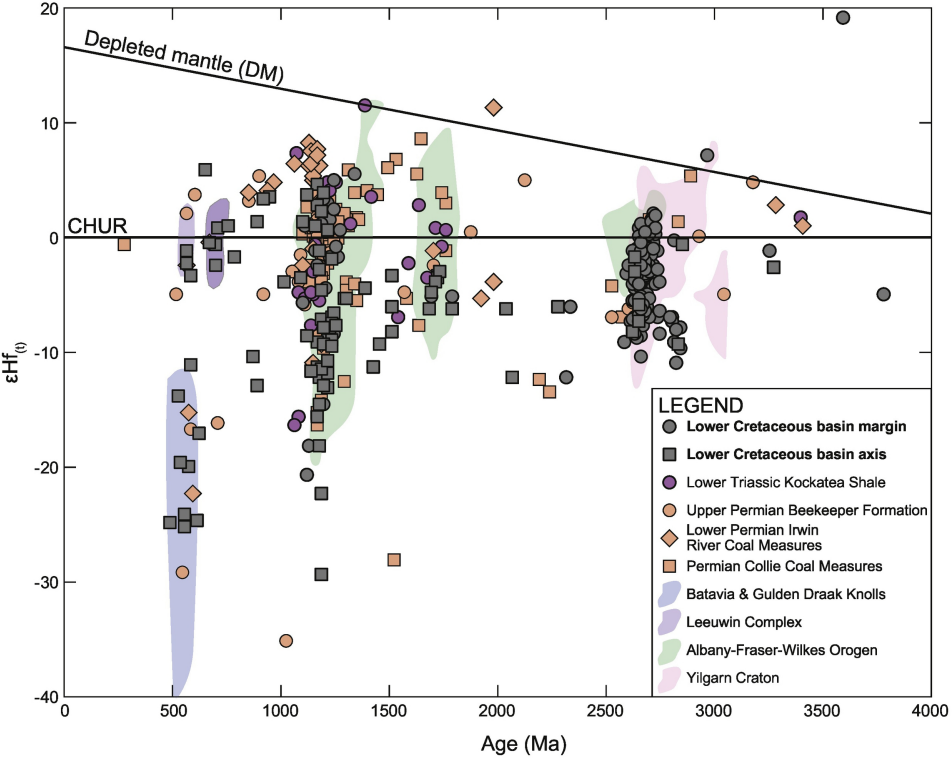
Depleted mantle (DM)
CHUR
εHf(t)
Age (Ma)
LEGEND
Lower Cretaceous basin margin
Lower Cretaceous basin axis
Lower Triassic Kockatea Shale
Upper Permian Beekeeper Formation
Lower Permian Irwin River Coal Measures
Permian Collie Coal Measures
Batavia & Gulden Draak Knolls
Leeuwin Complex
Albany-Fraser-Wilkes Orogen
Yilgarn Craton

Figure 6

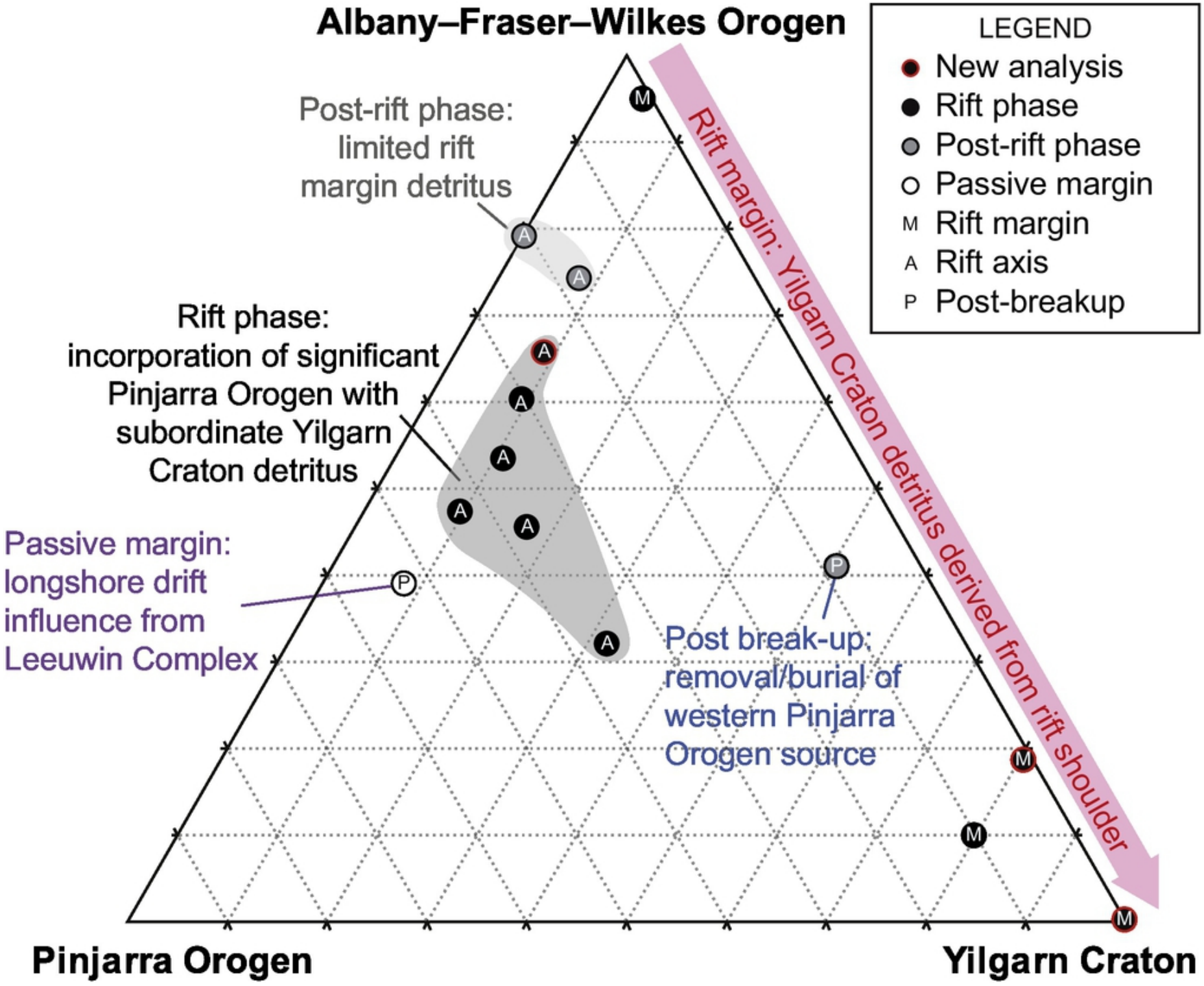
Albany–Fraser–Wilkes Orogen
LEGEND
New analysis
Rift phase
Post-rift phase
Passive margin
M Rift margin
A Rift axis
P Post-breakup
Post-rift phase: limited rift margin detritus
Rift phase: incorporation of significant Pinjarra Orogen with subordinate Yilgarn Craton detritus
Passive margin: longshore drift influence from Leeuwin Complex
Post break-up: removal/burial of western Pinjarra Orogen source
Rift margin: Yilgarn Craton detritus derived from rift shoulder
Pinjarra Orogen
Yilgarn Craton

Figure 7

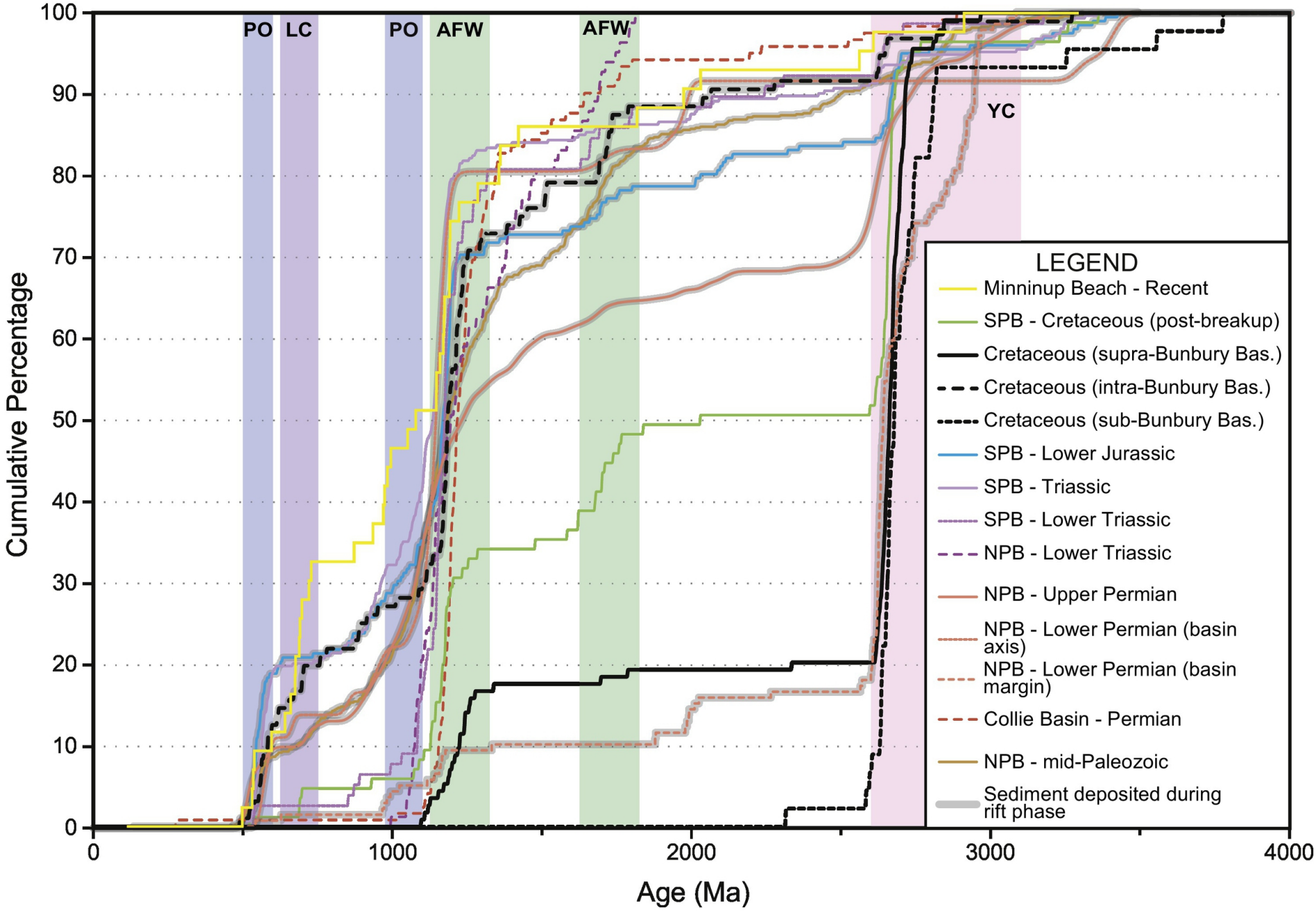
PO
LC
PO
AFW
AFW
YC
Cumulative Percentage
Age (Ma)
0
10
20
30
40
50
60
70
80
90
100
0
1000
2000
3000
4000
LEGEND
Minninup Beach - Recent
SPB - Cretaceous (post-breakup)
Cretaceous (supra-Bunbury Bas.)
Cretaceous (intra-Bunbury Bas.)
Cretaceous (sub-Bunbury Bas.)
SPB - Lower Jurassic
SPB - Triassic
SPB - Lower Triassic
NPB - Lower Triassic
NPB - Upper Permian
NPB - Lower Permian (basin axis)
NPB - Lower Permian (basin margin)
Collie Basin - Permian
NPB - mid-Paleozoic
Sediment deposited during rift phase

Figure 8

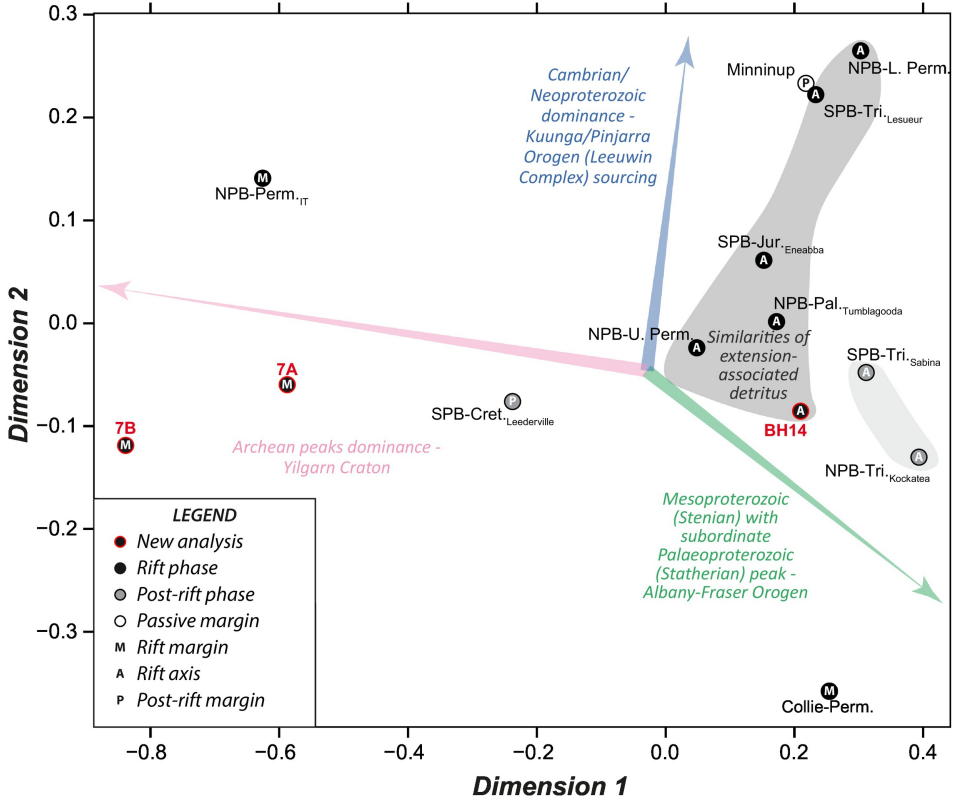
Dimension 2
Dimension 1
0.3
0.2
0.1
0.0
−0.1
−0.2
−0.3
−0.8
−0.6
−0.4
−0.2
0.0
0.2
0.4
Cambrian/ Neoproterozoic dominance - Kuunga/Pinjarra Orogen (Leeuwin Complex) sourcing
Minninup
NPB-L. Perm.
SPB-Tri.Lesueur
NPB-Perm.IT
SPB-Jur.Eneabba
NPB-Pal.Tumblagooda
NPB-U. Perm.
Similarities of extension-associated detritus
SPB-Tri.Sabina
7A
SPB-Cret.Leederville
BH14
7B
Archean peaks dominance - Yilgarn Craton
NPB-Tri.Kockatea
Mesoproterozoic (Stenian) with subordinate Palaeoproterozoic (Statherian) peak - Albany-Fraser Orogen
Collie-Perm.
LEGEND
New analysis
Rift phase
Post-rift phase
Passive margin
M Rift margin
A Rift axis
P Post-rift margin

Figure 9

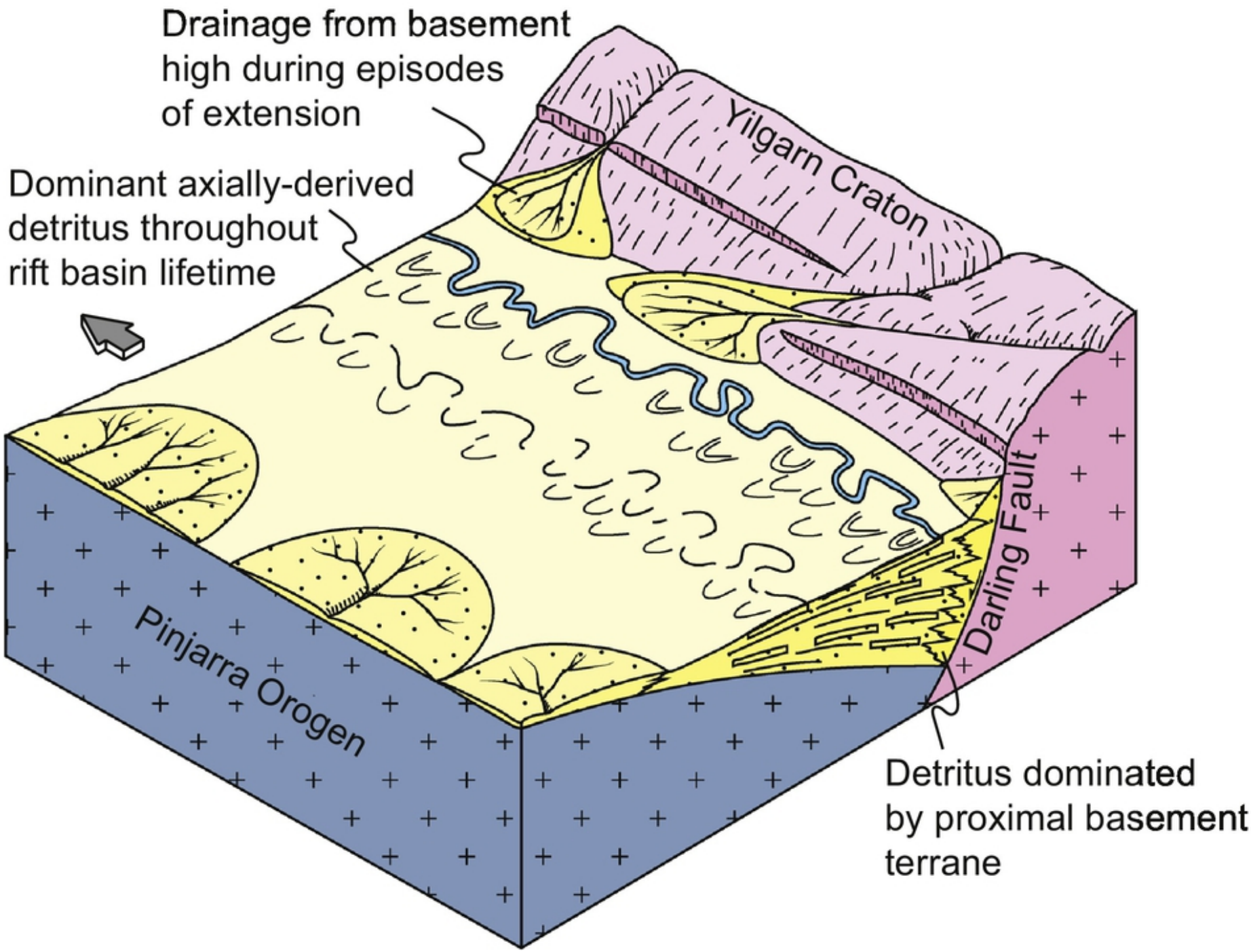
Drainage from basement high during episodes of extension
Dominant axially-derived detritus throughout rift basin lifetime
Yilgarn Craton
Darling Fault
Pinjarra Orogen
Detritus dominated by proximal basement terrane

Figure 10